UNIVERSIDADE DE SÃO PAULO
Escola de Engenharia de São Carlos

Aeroelastic Analysis of a Lightweight Topology-Optimized Sandwich Panel

Maliheh Najafi

Corrected thesis (Doctorate) - Postgraduate Program in Mechanical Engineering

Area of concentration: Dynamics and Mechatronics

EESC · USP

UNIVERSITY OF SÃO PAULO
SÃO CARLOS SCHOOL OF ENGINEERING

Maliheh Najafi

Aeroelastic analysis of a lightweight topology-optimized sandwich panel

São Carlos

2023

Maliheh Najafi

Aeroelastic analysis of a lightweight topology-optimized sandwich panel

Doctorate thesis presented to the São Carlos School of Engineering, University of São Paulo, to obtain the title of Doctorate in Sciences - Graduate Program in Mechanical Engineering. Area of concentration: Dynamics and Mechatronics.

Advisor: Prof. Assoc. Flávio Donizeti Marques

São Carlos

2023

FOLHA DE JULGAMENTO

Candidata: Bacharel **MALIHEH NAJAFI.**

Título da tese: "Análise aeroelástica de painel sanduíche da baixo peso de topologia otimizada.".

Data da defesa: 27/09/2023.

Comissão Julgadora	**Resultado**
Prof. Associado Flavio Donizeti Marques (Orientador) (Escola de Engenharia de São Carlos/EESC-USP)	APROVADO
Prof. Dr. António Joaquim Mendes Ferreira (Faculdade de Engenharia da Universidade do Porto/FEUP-Portugal)	APROVADO
Prof. Dr. Thiago Augusto Machado Guimarães (Universidade Federal de Uberlândia/UFU)	APROVADO
Prof. Titular Jonas de Carvalho (Escola de Engenharia de São Carlos/EESC-USP)	Aprovado!
Prof. Doutor Ricardo de Medeiros (Universidade do Estado de Santa Catarina/UDESC)	APROVADO

Coordenador do Programa de Pós-Graduação em Engenharia Mecânica:
Prof. Associado **Adriano Almeida Gonçalves Siqueira**

Presidente da Comissão de Pós-Graduação:
Prof. Titular **Carlos De Marqui Junior**

Este trabalho é dedicado aos alunos da USP, como uma contribuição das Bibliotecas do Campus USP de São Carlos para o desenvolvimento e disseminação da pesquisa científica da Universidade.

ACKNOWLEDGEMENTS

I would want to sincerely thank everyone who helped me finish my doctoral thesis. My sincere gratitude goes out to Professor Flávio Marques, my academic advisor, for all of his help and support during this challenging road. His insightful criticism and knowledge helped to mold our study.

In order to make this research possible, I would like to thank the financial support of the PrInt USP/CAPES program, Brazil (grant #88882.379170/2019-01).

I am grateful for my family's and friends' support and believe in me; they have been a great source of inspiration. Also, I would want to express my gratitude to all of the research subjects and others who shared their knowledge and experiences with this study. Your help was crucial to finishing this thesis.

In closing, I want to express my deepest gratitude to my little daughter, Maya, for her unwavering support and understanding during my challenging Ph.D. journey.

"Science is the light that illuminates the path of human progress, leading us towards a future full of possibility and wonder."

Hafez

ABSTRACT

Najafi, M. **Aeroelastic analysis of a lightweight topology-optimized sandwich panel**. 2023. 80p. PhD Dissertation (Doutorate) , São Carlos School of Engineering, University of São Paulo, São Carlos, 2023.

Sandwich structures with lattice cores are novel, lightweight composite structures and are widely used in the aerospace industry. Besides, the aeroelastic behavior of sandwich panels in a supersonic flow regime still needs to be thoroughly studied. This work is devoted to investigating the flutter properties of a sandwich panel whose core is inspired by the topology optimization method in supersonic airflow. In addition, an analytical model of the topology-optimized core sandwich panel employing layerwise theory and the homogenization approach is given for modal analysis. A three-layer continuum is applied to the entire sandwich panel, with the topology-optimized core being homogenized as an equivalent orthotropic layer based on an energy method. The first-order shear deformation theory in each layer is assumed, and displacement continuity is imposed at the layer interfaces. These assumptions constitute the foundation of the layerwise theory provided in this study. The supersonic Piston theory evaluates aerodynamic pressure. For the panel, a four-node Lagrangian quadrilateral element with nine degrees of freedom per node is employed. By comparing natural frequencies and mode shapes with those produced from commercial software and previous results in the literature, the accuracy and dependability of the new method are confirmed. On critical dynamic pressure, the effects of geometric parameters and material characteristics are explored. The results show that the proposed metastructure has the ability to use as a lightweight core sandwich panel in comparison to an isotropic panel and isotropic core sandwich panel in aircraft design, which leads to improving the efficiency of flight and is useful in the research of lightweight sandwich materials.

Keywords: Sandwich structures, lattice core, aeroelastic analysis, supersonic flutter, topology optimization method, layerwise finite element theory, homogenization approach, modal analysis, lightweight material.

RESUMO

Najafi, M. **Análise aeroelástica de um painel sanduíche leve com topologia otimizada**. 2023. 80p. PhD Dissertação (Doutorado) - Escola de Engenharia de São Carlos, Universidade de São Paulo, São Carlos, 2023.

Estruturas sanduíche com núcleos treliçados são novas estruturas compostas e têm sido amplamente utilizadas nas áreas aeroespacial e aeronáutica devido ao seu excelente desempenho, mas seus comportamentos aeroelásticos não foram totalmente estudados. Este trabalho é dedicado a investigar as propriedades de flutter de um painel sanduíche cujo núcleo é inspirado no método de otimização topológica em fluxo de ar supersônico. Além disso, um modelo analítico do painel sanduíche de núcleo otimizado para topologia empregando a teoria em camadas e a abordagem de homogeneização é fornecido para análise modal. Um contínuo de três camadas é aplicado a todo o painel sanduíche, com o núcleo otimizado de topologia sendo homogeneizado como uma camada ortotrópica equivalente com base em um método de energia. A teoria da deformação por cisalhamento de primeira ordem em cada camada é assumida e a continuidade do deslocamento é imposta nas interfaces das camadas. Essas suposições constituem a base da teoria de camadas fornecida neste estudo. A teoria do pistão supersônico avalia a pressão aerodinâmica. Para o painel, é empregado um elemento quadrilátero Lagrangeano de quatro nós com nove graus de liberdade por nó. Ao comparar frequências naturais e formas de modo com aquelas produzidas a partir de software comercial e resultados anteriores na literatura, a precisão e confiabilidade do novo método são confirmadas. Na pressão dinâmica crítica, os efeitos de parâmetros geométricos e características do material são explorados. Os resultados mostram que a metaestrutura proposta tem a capacidade de ser usada como um painel sanduíche de núcleo leve em comparação com um painel sanduíche de núcleo isotrópico e um painel sanduíche de núcleo isotrópico no projeto de aeronaves, o que leva a melhorar a eficiência de voo e é útil na pesquisa de painéis sanduíche leves materiais.

Palavras-chave: Estruturas sanduíche, núcleo treliçado, análise aeroelástica, flutter supersônico, método de otimização topológica, teoria dos elementos finitos em camadas, abordagem de homogeneização, análise modal, material leve.

LIST OF FIGURES

LIST OF TABLES

LIST OF ABBREVIATIONS AND ACRONYMS

FEM	Finite Element Method
TOP	Topology Optimization Method
DOF	Degree Of Freedom
LCO	Limit Cycle Oscillation
SIMP	Solid Isotropic Material Penalization
ESO	Evolutionary Structural Optimization
LSM	Level Set Method
PVW	Principle of Virtual Work
CSP	Composite Sandwich Panel
RVE	Representative Volume Element
SSSS	Simply Supported at all Sides

LIST OF SYMBOLS

A	Cross sectional area
$\mathbf{A}$	Aerodynamic force matrix
A_x	Actual section area of the corrugated core sheet
A_{eq_x}	Section area of the equivalent material
A_c	Area, per unit width, of corrugation cross section perpendicular to corrugation axis
b	Plate's weight
c	Compliance
$\mathbf{C}_{total}$	Stiffness matrix quantities of the total panel
$\mathbf{C}_1$	Stiffness matrices of the bottom face
$\mathbf{C}_2$	Stiffness matrices of the top face
$\mathbf{C}_c$	Equivalent stiffness of the core
E	Young's modulus
E_e	Young's modulus of element
E_0	Stiffness of the material
E_{min}	Very small stiffness
E_y	Elastic modulus in y-direction
E_x	Elastic modulus in x-direction
E^f	Young modulus of the face sheet
$F(u(\rho), \rho)$	Objective function
f_A	Aerodynamic force vector
f	Prescribed volume fraction
G	Shear modulus
g_a	Damping factor

$\mathbf{G}(\lambda)$	Global damping matrix
G_{yz}	Transverse shear modulus in yz plane
G_{xz}	Transverse shear modulus in xz plane
G_{xy}	In-plane shear modulus
G_c	Shear modulus of elasticity of core material
G_f	Shear modulus of the face sheet material
h	Plate's thickness
H	Core thinkness
h_{iso}	Iisotropic panel's thickness
I	Second moment of area
K	Bulk modulus
k_0	Element stiffness matrix
$\mathbf{K}$	Global stiffness matrix
k	Shear factor
k_{eq12}	Equivalent spring constant of segments one and two
k_{eq34}	Equivalent spring constant of segments three and four
l_1	Length of segments one
l_2	Length of segments two
L	Plate's length
m	Number of constraints
M_∞	Mach number
$\mathbf{M}$	Mass matrix
M_0	Moment
N	Number of elements used to discretize the design domain
T	Inner force
$N_i(\zeta, \eta)$	Shape functions

p	Penalization factor
q_∞	Free-stream dynamic pressure
$Q_p^{(k)}$	Constitutive matrices for the $k^{(th)}$ layer
$Q_s^{(k)}$	Constitutive matrices for the $k^{(th)}$ layer
S	Panel area
T	Kinetic energy
t_1	Bottom face thickness
t_2	Top face thickness
t_c	Thickness of corrugated-core sheet
t_f	Thickness of each face sheet
$u(p)$	Design space
U_∞	Velocity
u_e	Element displacement vector
u_0, υ_0	Membrane DOFs
u	Inplane displacements at any point (x, y, z)
U	Strain energy function
$\mathbf{U}$	Vector of the global degrees of freedom
U_a	Velocity of air
$\mathbf{U}$	Global displacement
$V(x)$	Material volume
V_0	Design domain volume
V	Vertical force
w	Transverse displacement field
W	Work done by the externally applied non-conservative load
x	Element densities
x_e	Density of each element

ν	Poisson's ratio
ν_{yx}	Poisson's ratio in the yx-plane
ν^f	Poisson's ratio of the face sheet
$\rho(u)$	Main design variable or material distribution
ρ	Panel's density
ρ_c	The equivalent density
ρ_a	Freestream air density
λ	Dimensionless dynamic pressure
λ_f	Critical dynamic pressure
Λ	Non-dimensional fundamental frequency
ΔP	Aerodynamic pressure
δ	Vector of degrees of freedom
δ_i	Generalized coordinates
ω_0	Reference frequency
ω	Deflection
ω	Natural frequency
υ_i	Transverse shear correction factors
υ_j	Transverse shear correction factors
υ	Inplane displacements at any point (x, y, z)
υ_0	Inplane displacement of the point (x, y, 0)
$\phi_x^{(1)}, \phi_y^{(1)}$	Rotation DOFs of the normals to the bottom layer about the y and x axes
$\phi_x^{(2)}, \phi_y^{(2)}$	Rotation DOFs of the normals to the midplane about the y and x axes
$\phi_x^{(3)}, \phi_y^{(3)}$	Rotation DOFs of the normals to the upper layer about the y and x axes
ε_p	In-plane strain
ε_s	Transverse shear strain

$\varepsilon^{mf(3)}$	Membrane-bending coupling components for layer 3
$\varepsilon^{mf(1)}$	Membrane-bending coupling components for layer 1
Ψ	Flow angle

CONTENTS

1 INTRODUCTION

Panel flutter is an increasingly serious problem that threatens aerospace vehicles' operational safety, flight performance, and energy efficiency. Its avoidance is always of vital importance before an episode occurs (NJUGUNA, 2007), and is a big challenge during the design stage. This phenomenon is a self-excited dynamic instability that arises in high airflow velocity passing on aircraft external skin structural elements (DOWELL, 1974; FUNG, 2008; BISPLINGHOFF; ASHLEY, 2013). This aeroelastic problem happens due to the interaction between aerodynamic, elastic, and inertia forces. The transverse vibrations of panels under the effect of supersonic aerodynamic pressure can increase in amplitude, which may lead to structural failure. This instability can happen in a catastrophic way leading to limit cycle oscillations and chaotic motions. Therefore, the panel flutter phenomenon prediction, prevention, and suppression are essential factors in the design of a new supersonic flight vehicle's skin.

This chapter starts by answering this question "with appearing metastructure in the industrial application as a new generation of composites, how can the core's geometry of a sandwich panel be designed to perform better in the aeroelastic application?". In the following, a review of the aeroelasticity of sandwich panels and the world of metastructures is done. In the next section, the topology optimization method is presented as the method to find the core of the sandwich panel. Also, to find the mechanical properties of the metastructure core the works related to the homogenization method are expressed.

1.1 Motivation

Modern aircraft requiring high speed with lightweight arrangement makes the aeroelastic panel flutter analysis a necessity in the design stage. As one of the significant requirements during the design stage of aerospace systems is choosing the optimum composite panels concerning lightweight and flutter behavior against aeroelastic problems, researchers and engineers are studying and using different types of composite structures in their designs to achieve the optimal performance and criterion to avoid skewing and cracking panels (WEI; YAM; CHENG, 2004; PIDAPARTI; CHANG, 1998; STRGANAC; KIM, 1996). Therefore, the motivation of this work is finding a sandwich panel to have a better performance in aeroelastic applications.

1.2 Literature review

1.2.1 Flutter in sandwich panels in supersonic regime

For the supersonic panel flutter problem, the possibility of accomplishing improvements ensures the potential of the sandwich panels. Although many investigations have focused on the mechanical behaviors of the sandwich panels with optimized cores, to the best of the author's knowledge, only a few studies have been done on their aeroelastic behavior. Castanié, Bouvet and Ginot (2020) conducts a review of composite sandwich structures used in aerospace applications. Song and Li (2016) studied the aerothermoelastic properties of sandwich composite panels with pyramidal truss and triangular grid cores in supersonic flow. An active flutter and buckling control theoretical analysis of a sandwich panel with a triangular lattice core was investigated under supersonic flow (SONG; LI, 2017). Moreover, Chai, Song and Li (2017) presented an investigation on the aerothermoelastic flutter analysis and thermal buckling control of sandwich panels with the pyramidal lattice core resting on elastic foundations in supersonic airflow. They analyzed the influences of the elastic foundation, aspect ratio, core-to-face sheet thickness ratio, and inclination angle of the core truss on the aerothermoelastic characteristics of the lattice sandwich panel numerically. Also, the only aeroelastic analysis of foam-filled composite corrugated sandwich plates was done recently (ZHUANG; YANG; WU, 2021). Furthermore, Zhang, Yan and Xia (2021) investigated the vibrations and flutter of a honeycomb sandwich plate with zero Poisson ratio under supersonic airflow. Therefore, developing innovative ways to improve the aeroelastic properties of aerospace high-speed vehicle panels is essential. These may base on in-depth physical insights into the panel flutter behavior of metastructure panels.

1.2.2 Metastructures

In recent years, a new generation of materials known as metamaterials and their possible arrangements as metastructures have been proposed continuously in aerospace applications. The prominent concept of metamaterials was introduced by Yu *et al.* (2018). Metastructures are human-made structures that consist of identical substructures or cells that have been implemented identically. These artificial materials enable engineers to design cell shapes for specific applications. Due to the periodic structural patterns, a metastructure exhibits advanced mechanical and physical properties such as negative Poisson ratio (auxetics meta structures), negative coefficient of thermal expansion, high energy absorption, vibration attenuation, and negative mass inertia, which are not accessible in natural materials. Compared to composites, their unique mechanical properties are based on spatial geometry instead of material composition (SHAMONINA; SOLYMAR, 2007; FINDEISEN *et al.*, 2017; WU *et al.*, 2019). Classification of mechanical metamaterials based on the Young modulus (E), shear modulus (G), bulk modulus (K), and the Poisson

ratio (ν) have been established to choose the structural topology based on stiffness, rigidity, and compressibility (YU *et al.*, 2018). In selecting cellular materials such as honeycombs, foams, and lattices, designers have been using the traditional engineering approaches, a biomimetic method, or a coupled of these two schemes (BHATE *et al.*, 2019).

Recently, metamaterials in industrial applications and investigations can be seen in re-configurable structures, morphing airfoil with chiral core configuration, chiral flexible electronics, and chiral sandwich panels (WU *et al.*, 2019). For the panel flutter problem, the possibilities of accomplishing improvements ensure the potential of the metastructure concept.

Some research contributions have been devoted to changing mechanical metamaterial properties to apply them for different purposes like elastic wave absorption with vibration suppression (HE; XIAO; LI, 2017; PENG; PAI; DENG, 2015), wave propagation (NOUH; ALDRAIHEM; BAZ, 2015), and vibration isolation and energy harvesting (LI *et al.*, 2017). These studies may provide some clues for the development of innovative metamaterial panels in high-speed aeroelastic applications.

1.2.3 Topology optimization

Aeroelastic optimization is a consolidated field in many aerospace research and industrial applications. Structural plates can be optimized based on some flutter requirements by computationally different strategies that introduce various forms of objective functions. In the design of plate structures, optimization (maximization) of flutter speed is a fundamental concept. Nevertheless, the formulation of the problem can be carried out in various ways. Muc and Flis (2019) applied the direct formulation of the aeroelasticity problem. Moreover, the implicit formulation with a bound was used for aeroelasticity optimization by Song *et al.* (2018) and Guo (2007). Li and Narita (2014) carried the maximization of the weighted sum of the critical aerodynamic pressures under different probability density functions of flow orientations. Moreover, the maximization of natural frequencies related to the vibration modes involved in the flutter phenomenon, called as aeroelastic optimization method by finite difference, was done by Leon *et al.* (2012) and Katsikadelis and Babouskos (2018). Maximization of a function of the panel stiffness, damping, and dynamic pressure values of the free stream was used by researchers (VIJAY; DURVASULA, 1998).

The sandwich panel with lattice core, in aerospace applications, was optimized with respect to the divergence or flutter behavior. The additional design variables introduced by the structure of sandwich constructions are directly connected with the form of mechanical properties of the core. As in metastructure sandwich panels, the core is a metamaterial, so the optimization algorithms can be used in defining grading functions. In this case, the topology optimization methods should be adopted for this class of problems (MUC; FLIS,

2019).

Topology optimization, as a mathematical approach, is a numerically iterative procedure to optimize the distribution of materials in a given design domain, subject to a specified objective function and constraint(s) to maximize the performance of the system (BENDSOE; SIGMUND, 2013), which often used in manufacturing industries. In the last decade, this method has made extraordinary development in architecting materials with novel properties (OSANOV; GUEST, 2016).

Bendsoe and Kikuchi (1988) proposed the basic theory of topology optimization, which replaces an optimization problem with a material distribution problem within a fixed design domain.

The number of articles on topology optimization in the aeroelastic application is rare. By considering aerodynamic loads, the topological design of internal wing ribs was studied by Krog *et al.* (2004). Moreover, Stanford and Beran (2011) and Leon *et al.* (2012) investigated the aeroelastic instability (i.e., flutter) in the topology optimization of cantilevered wing structures. Stanford and Beran (2013) optimized the aerothermoelastic panels for flutter and buckling matrices by topology optimization method. Moreover, the effect of various constraint boundaries, temperature gradients, and thermal load magnitude was analyzed.

The general form of a topology optimization problem is written as (SIGMUND; MAUTE, 2013),

$$\text{minimize} : F = F(u(\rho), \rho) = \int_{\Omega} f(u(\rho), \rho) dV \quad , \tag{1.1}$$

$$\text{subject to} \;\; G_0(\rho) = \int_{\Omega} \rho(x) dV - V_0 \leq 0 \quad , \tag{1.2}$$

$$G_j(u(\rho), \rho) \leq 0 \;\; \text{with} \;\; j = 1, ..., m \quad , \tag{1.3}$$

$$\rho(x) = 0 \;\; \text{or} \;\; 1, \forall x \in \Omega \tag{1.4}$$

which its aim is finding the material distribution that minimizes an objective function $F(u(\rho), \rho)$, subject to a volume constraint G_0 and perhaps a number of additional constraints G_j and m is the number of constraints. $u(\rho)$ is the design space and $\rho(x)$ is the main design variable or material distribution, which can have a value of 0 (void) or 1 (solid material) at any point in the design domain.

Each problem possesses different objective functions. Commonly, the most used one is minimizing compliance, or in other words, maximizing the stiffness of the structure. There exist several classifications of topology optimization methods, such as the homogenization method (BENDSOE; KIKUCHI, 1988), the solid isotropic material with penalization (SIMP) method, the evolutionary structural optimization (ESO) method and the level set method (LSM) (GAO *et al.*, 2019). A combination of the topology optimization method

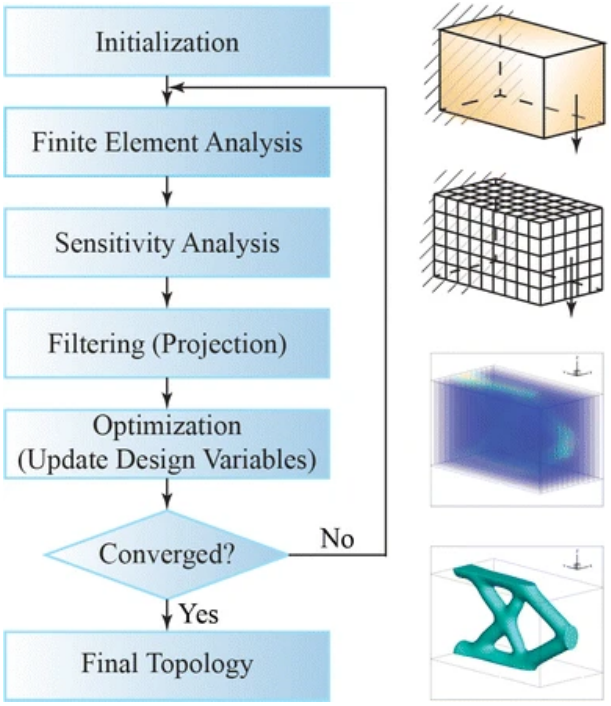

Figure 1 – Topology optimization flowchart (SUTRADHAR *et al.*, 2016).

with the homogenization method to optimize the microstructure was proposed (GUEDES; KIKUCHI, 1990; SIGMUND, 1994; CLAUSEN *et al.*, 2015).

There were several works for the optimization of metamaterials. An optimization approach of material concerning nonlinear properties (CLAUSEN *et al.*, 2015; WANG; SIGMUND; JENSEN, 2014) with the programmable Poisson ratio and subsequent shape optimization to attain any given Poisson ratio was studied in 3D auxetic microstructures (WANG, 2018). Another method to optimize auxetic microstructures implies the parametric level set approach (WANG *et al.*, 2014).

The finite element method (FEM) has been applied dominantly to perform numerical analysis in topology optimization problems. Several reasons demonstrate that in the design of auxetic microstructures, the FEM is one factor to affect the effectiveness of the topology optimization. Firstly, the finite element mesh is just an approximation of the initial configuration of the design domain, which lessens the numerical accuracy. Further, the lower-order continuity of the responses between the nearby finite elements, although the higher-order finite elements are employed. Furthermore, the lower efficiency in accomplishing a finite element mesh with high quality (GAO *et al.*, 2019).

An effective and efficient topology optimization method for designing metamaterials in aeroelasticity applications is still in demand. One part of this proposal is motivated to develop an optimization method with topology analysis (SIGMUND, 2001) for supersonic panel flutter metastructure in flutter point to find the internal geometry of the panel.

1.2.4 Homogenization methods

In recent years, with the advancement of technology, composite materials have been increasing in industrial applications such as mechanical, aerospace, civil, transportation, marine engineering, medicine, sports, recreational goods, and others. Composite materials may be defined as man-made materials with specific unit cell geometry. The mechanical and physical properties of a composite are different from their individual constituents. One way of finding the properties of such composites is by carrying out experimental tests. As the cost of tests of this media with a large heterogeneity is high, a natural way to overcome this difficulty is to replace the composite with a kind of equivalent material model. This procedure is usually called homogenization, which is an efficient way to determine the effective material properties of composite materials. Figure 2 shows a schematic of the homogenization method of a metastructure cantilever beam.

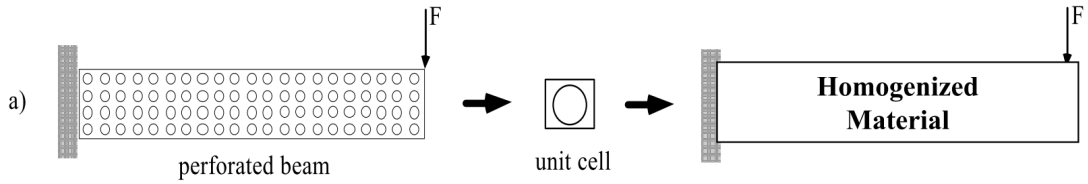

Figure 2 – Schematics of the homogenization method.

As the core geometry strongly affects the mechanical properties and thus those of the equivalent material, the micromechanical analysis of composite materials has been investigated for many years. Cheng, Lee and Lu (2006) estimated elastic constants of sandwich structures with various cores by an analytical formula. Furthermore, Wang and Chung (2011) studied the properties of triangular corrugation. The critical loads for different failure mechanisms on the structural performance of triangular panels and also the diamond corrugation shapes were studied in two investigations (VALDEVIT; HUTCHINSON; EVANS, 2004; VALDEVIT *et al.*, 2006).

Several authors studied the mechanical properties of trapezoidal geometries (LIBOVE; HUBKA, 1951; SAMANTA; MUKHOPADHYAY, 1999). Bartolozzi, Baldanzini and Pierini (2014) developed a general analytical formulation to calculate the equivalent properties of corrugated cores of sandwich structures, which is mainly based on an energetic approach, starting from Castigliano's second theorem. In this research, this method, with some modifications, is used to calculate the equivalent mechanical properties of the suggested structure.

1.3 Objectives

Sandwich structures with lattice cores are innovative composite structures that have found extensive usage in the aerospace and aviation industries because of their

great performance. However, their aeroelastic behaviors have not yet been thoroughly investigated. The original contribution of my work to the state of the art includes the analysis of a new sandwich panel whose core is inspired by the topology optimization method that significantly improves the flutter boundary in supersonic airflow applications. The entire sandwich panel is modeled as a three-layer continuum, with the energy-based homogenization of the topology-optimized core as an analogous orthotropic layer. It is assumed that each layer follows the first-order shear deformation theory, and the layer interfaces are forced to follow displacement continuity. Unsteady aerodynamic pressure is assessed using the supersonic piston theory. A Lagrangian quadrilateral element with four nodes and nine degrees of freedom per node is used for the panel.

To verify the precision and reliability of the novel technique, natural frequencies, and mode shapes are compared to those generated by commercial software and earlier findings in the literature. The influence of geometrical variables and material properties is examined on critical dynamic pressure. The aeroelastic characteristics of the lightweight core sandwich panel with an isotropic panel and the isotropic core sandwich panel are compared, thereby contributing to understanding the efficacy of this structure in enhancing flight efficiency.

1.4 Thesis statement

The aeroelastic analysis of topology-optimized sandwich panels is divided into four other chapters in addition to this introduction. The theories behind the homogenization approach and topology optimization are presented in Chapter 2. The structural model, aerodynamic model, finite element discretization, final aeroelastic equation of motion, flutter analysis, and solution methods are all presented in Chapter 3. Homogenization technique validation and layerwise theory validation are included in the model validation presented and discussed in Chapter 4. The accuracy of the 3D model is verified by comparing the dimensionless frequency in the references and the first six natural frequencies (vibration modes) between 3D-FEM and 3D-ABAQUS models under simple-supported boundary conditions. Linear flutter analysis of the topology-optimized core sandwich panel, panel modes, and flutter modes is also investigated in this chapter.

Additionally, the impacts of face-to-thickness ratio, flow angle, TOP metastructure angle, and core metastructure thickness are examined. A comparison of isotropic panels, isotropic sandwich panels, and TOP sandwich panels is completed at the end of this section. In addition to summarizing this study's key results and findings, Chapter 5 offers recommendations for further research. The workflow of the aeroelastic analysis of the TOP sandwich panel is shown in Figure 3. To some up, it is shown that the advantage of the proposed sandwich panel with topology optimized core is the ability to be used as a lightweight core sandwich panel in aircraft designing, which leads to improved flight

efficiency. Moreover, its critical flutter boundary and density show the superior aeroelastic properties of the sandwich panel.

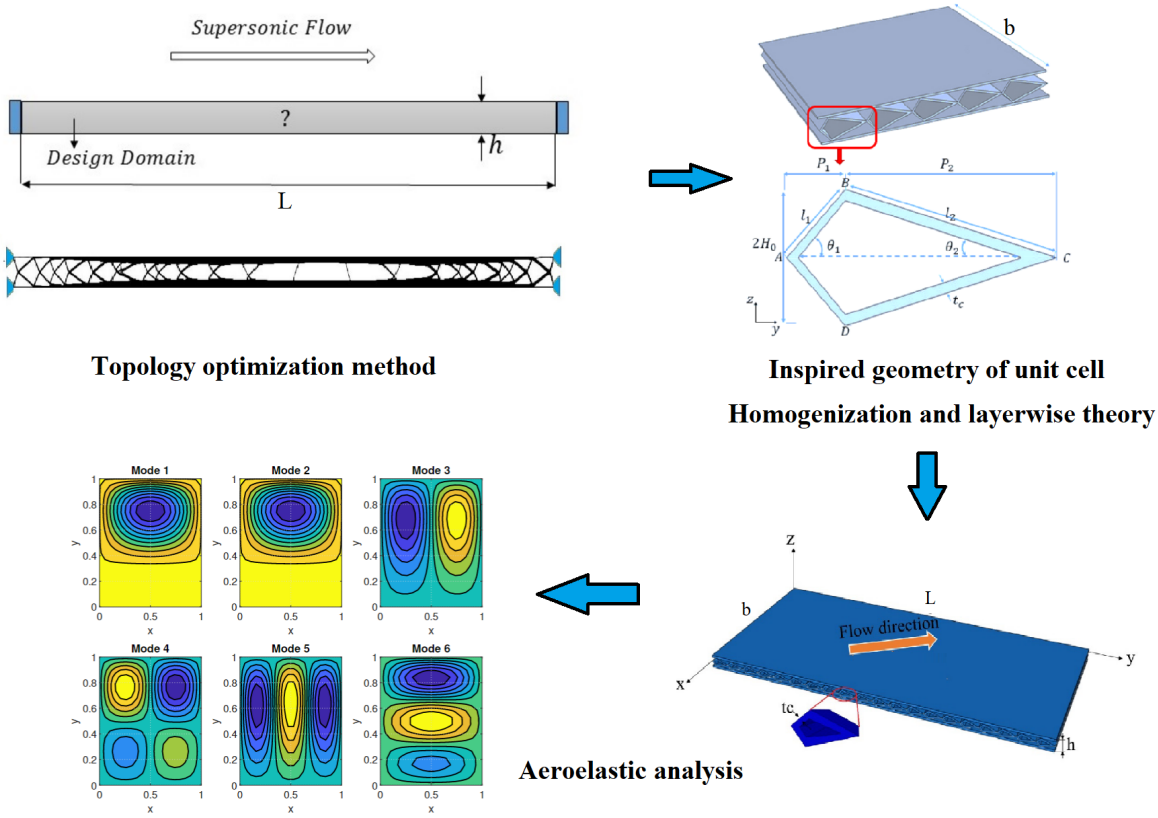

Figure 3 – The flowchart of the aeroelastic analysis of the TOP core sandwich panel.

2 TOPOLOGY OPTIMIZATION AND HOMOGENIZATION METHOD

In the field of high-speed aeroelasticity applications, it is challenging to propose a metamaterial structure as a core of the panels to enhance the panel flutter behavior, such as critical flutter speed, critical dynamic pressure, maximum limit cycle oscillation amplitude, and the post-flutter regime. From an engineering point of view, the four elastic constants of common mechanical metamaterials are Young's modulus (E), shear modulus (G), bulk modulus (K) and the Poisson's ratio (ν). The first three measure the stiffness, strength, and compressibility of structural material.

In this study, it is proposed a compliance Topology Optimization (TO) in order to find the metastructure geometry of the panel.

An essential characteristic of an aeroelastic system is its flutter boundary, or stability boundary, which is the critical condition for limit cycle oscillations that start to occur from this point. In the following, the flutter boundary is calculated for an isotropic panel with bellow characteristics in the simply supported boundary condition.

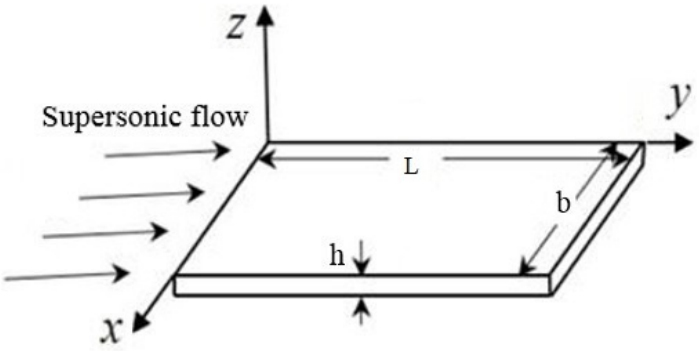

Figure 4 – Illustration of the supersonic panel flutter problem setup.

Consider a plate ($L \times b$) with thickness h, in which the length-to-thickness ratio is $L/h = 10$. The edges are aligned with the x and y-directions, respectively, as depicted in Figure 4. Moreover, the air flows over the panel's upper surface at supersonic speed ($M = 2$) and along the positive y direction. The flow generates an aerodynamic pressure ΔP that acts normally to the panel surface, thus causing it to deform and can be calculated within good accuracy through first-order piston theory (BISMARCK-NASR, 1976) as:

$$\Delta P(w(x,y,t)) = -\frac{2q_\infty}{\sqrt{M_\infty^2 - 1}}\left[\frac{\partial w}{\partial y} + \left(\frac{M_\infty^2 - 2}{M_\infty^2 - 1}\right)\frac{1}{U_\infty}\frac{\partial w}{\partial t}\right] \quad , \tag{2.1}$$

where w is the transverse displacement field of the plate, q_∞ is the free-stream dynamic pressure, M_∞ is the Mach number, and U_∞ is the velocity.

Equation (2.1) can be rewritten as:

$$\Delta P = -\lambda(\frac{D}{L^3})\frac{\partial w}{\partial y} - g_a(\rho h w_0)\frac{\partial w}{\partial t} \quad , \tag{2.2}$$

where ρ, h and L are the panel's density, thickness, and length, respectively, and:

$$\begin{cases} D = \frac{Eh^3}{12(1-\nu^2)} \\ w_0 = \sqrt{\frac{D}{\rho h L^4}} \\ \lambda = \frac{2q_\infty L^3}{D\sqrt{M_\infty^2-1}} \\ g_a = \sqrt{\frac{\lambda\mu}{\sqrt{M_\infty^2-1}}}(\frac{M_\infty^2-2}{M_\infty^2-1}) \simeq \sqrt{\frac{\mu\lambda}{M_\infty}} \\ \mu = \frac{L\rho_\infty}{h\rho} \end{cases} , \tag{2.3}$$

where E and ν are the Young modulus and Poisson ratio of the panel, ω_0 is the reference frequency, λ is dynamic pressure, and g_a is the damping factor.

The Mindlin plate theory is used for the plate. Moreover, the equations of motion are derived through the Principle of Virtual Work (PVW), which yields the aeroelastic equations of motion. For more details, the reader is referred to the work by Pacheco, Ferreira and Marques (2018), and by dropping the nonlinear stiffness, the value of λ_f can be obtained by solving the linear problem:

$$\mathbf{M}\ddot{\mathbf{U}} + \mathbf{G}(\lambda)\dot{\mathbf{U}} + \mathbf{K}(\lambda)\mathbf{U} = \mathbf{0} \quad , \tag{2.4}$$

where $\mathbf{M}$ is the mass matrix, $\mathbf{G}(\lambda)$ is the global damping matrix, $\mathbf{K}$ is the stiffness matrix, and $\mathbf{U}$ is the vector of the global degrees of freedom.

For dimensionless dynamic pressure (λ) below the flutter boundary (λ_f), the system after some vibrations, gradually returns to its static equilibrium. So, the behavior of the panel in $\lambda < \lambda_f$ can be considered a linear problem.

As illustrated in Table 1, the analysis of flutter boundary results have been generated for an isotropic panel, within simply supported boundary condition, and the geometric and material parameters are: $L = b$, $\frac{L}{h} = 10$, $E = 110GPa$, $\nu = 0.34$ and $\rho = 4.3\frac{g}{cm^3}$, which are the properties of Ti6A14V alloy.

Table 1 – Flutter boundary for the isotropic panel in the simply supported boundary condition.

Boundary condition	λ_f
Simply-Supported	483

The aerodynamic force at flutter condition based on the critical dimensionless dynamic pressure, λ_f, is calculated. Since for $\lambda < \lambda_f$ the panel is expected to display damped motion, and after some perturbations, it gradually returns to static condition, so

by omitting the aerodynamic damping term the Equation (2.1) can be reduced to steady piston theory formulation:

$$\Delta P(w(x,y)) = -\frac{2q_\infty}{\sqrt{M_\infty^2 - 1}}\left(\frac{\partial w}{\partial y}\right) \quad . \tag{2.5}$$

By estimating the equation of displacement of the panel, the aerodynamic pressure and as a result, the aerodynamic force on the panel in the critical flutter point are found. The Figure 5 indicates the fluttering shape at $\lambda_f = 483$ for the simply supported isotropic panel.

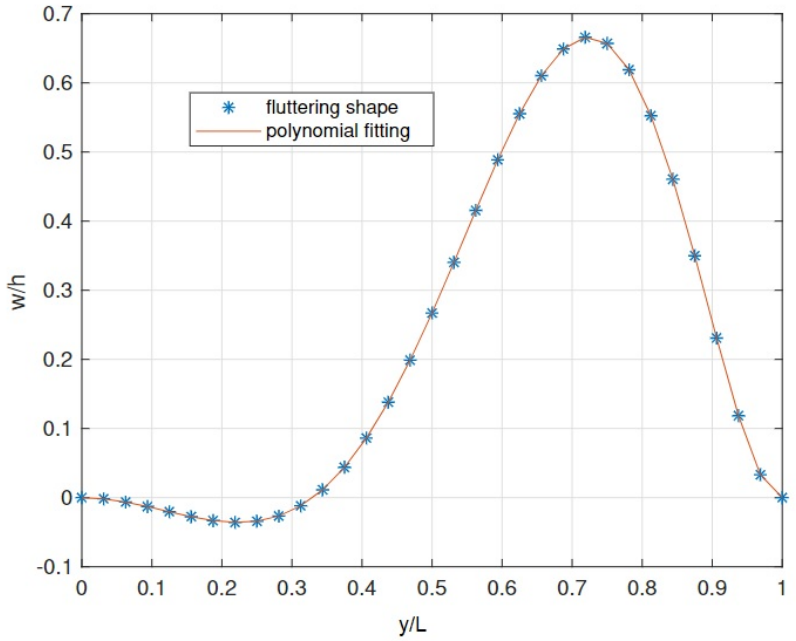

Figure 5 – Mid-section transverse displacement in y-direction for the simply supported isotropic panel.

The fitting equation to estimate the non-dimensional displacement is:

$$\begin{aligned} w/h(y/L) \quad &= \quad p_1(y/L)^7 + p_2(y/L)^6 + p_3(y/L)^5 + \\ &\quad + p_4(y/L)^4 + p_5(y/L)^3 + p_6(y/L)^2 + p_7(y/L) + p_8 \quad , \end{aligned} \tag{2.6}$$

where: $p_1 = 47.911$, $p_2 = -88.733$, $p_3 = 28.965$, $p_4 = 16.77$, $p_5 = -4.6626$, $p_6 = -0.13258$, $p_7 = -0.11605$, $p_8 = 0.0010925$.

The net aerodynamic force can be estimated to insert in the topology optimization method:

$$f_A = \Delta P(w(x,y))S \quad , \tag{2.7}$$

where S is the panel area.

In the design stage of any structural component in aerodynamic applications, a panel's weight should be as low as possible so that the system's physical response is acceptable. In order to reach this goal, there are two ways:

1. the minimum mass of a thin panel under a flutter constraint;

2. the maximum flutter speed under a mass constraint.

In this research, our purpose is to minimize the weight of the panel in the flutter boundary, which leads to an increase in the efficiency of aerospace vehicles. This section analyses topology optimization of a two-dimensional isotropic panel based on the SIMP (solid isotropic material with penalization) method (BENDSØE, 2003) subjected to aerodynamic, inertial, and elastic loads statically.

The topology optimization is applied to the aeroelastic model of the isotropic panel structure. The panel comprises a two-dimension plate with length L and thickness $h = L/10$, which is required to study the internal topology of the structure, with support in both ends, where an external side is under the supersonic flow field's effects, Figure 6. The structure is assumed to be infinitely long in the third dimension.

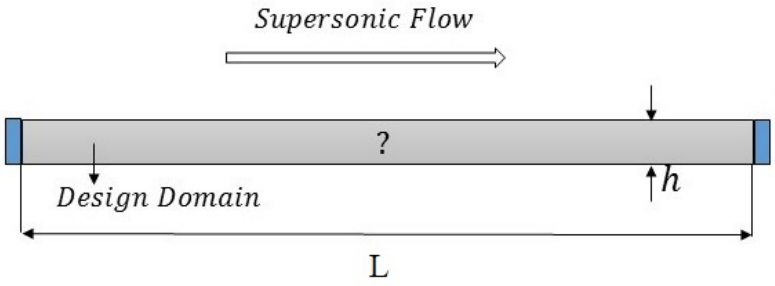

Figure 6 – Illustration of the supersonic panel flutter problem setup and design domain

The design domain is discretized into finite square elements, and the vector of design variables is the density of each element x_e, which smoothly varies between 0 (void) and 1 (solid). The upper surface, which is subjected to high-speed supersonic flow, and the lower surface are fixed as solid. The remainder constitutes the design domain. In the topology optimization method, the linear steady finite element solution is used on the panel (FERRARI; SIGMUND, 2020). In this study, the mathematical formulation of the optimization problem is based on a modified SIMP approach (ANDREASSEN *et al.*, 2011), where the objective is to minimize the compliance under flutter conditions which can be written as:

$$\begin{gathered} min(x) : c(x) = U^T K U = \sum_{e=1}^{N} E_e(x_e) u_e^T k_0 u_e \\ \text{subject to: } V(x)/V_0 = f \\ \mathbf{KU} = \mathbf{f}_A \\ 0 \leq x \leq 1 \end{gathered} \quad , \tag{2.8}$$

where c is the compliance, $\mathbf{U}$ is the global displacement, $\mathbf{f}_A$ is the aerodynamic force vector, $\mathbf{K}$, k_0, and u_e are the global stiffness matrix, the element stiffness matrix for an element

with unit Young's modulus and the element displacement vector, respectively, x as the element densities is the vector of design variables, N is the number of elements used to discretize the design domain, $V(x)$ and V_0 are the material volume and design domain volume, respectively, and f is the prescribed volume fraction. Each element e is assigned a density x_e that determines its Young's modulus E_e. The parameter E_e is defined as,

$$E_e(x_e) = E_{min} + x_e^p(E_0 - E_{min}), 0 \leq x_e \leq 1 \quad , \tag{2.9}$$

where E_0 is the stiffness of the material, E_{min} is a very small stiffness assigned to void regions in order to prevent the stiffness matrix from becoming singular, and p is a penalization factor introduced to ensure black-and-white solutions.

Figure 7 shows the topology optimization of the two dimensions simply supported panel at both ends on the flutter boundary. It displays that at the three-quarter of the panel, the topology is thicker and the density of the internal topology of the panel is higher than other parts.

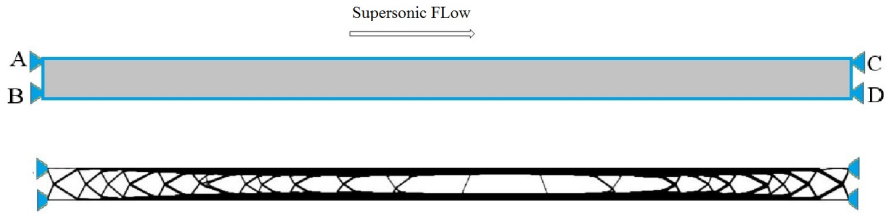

Figure 7 – Topology optimization of the simply supported panel in flutter boundary

In the following, the lightweight metastructure panel is designed based on the microstructure of the topology-optimized panel in flutter condition, as shown in Figure 8. Equivalent parameters need to be computed for the structure. The general analytical method is applied to calculate the equivalent mechanical properties of the core (BARTOLOZZI; BALDANZINI; PIERINI, 2014). However, to represent geometries that are symmetrical about the horizontal axis, such as x cores, this method is inadequate and is only useful for homogenizing corrugated cores like triangular, circular, or sinusoidal shapes as the middle layer of the CSP. Modifications need to be made to such a homogenization method when applying it to the TOP core sandwich panel considering the upper part and lower part of the unit cell behave like two parallel springs.

The unit cell of the metastructure panel, the reference system, and geometrical parameters are displayed in Figure 8. The y-axis denotes the array direction of the unit cell, while the z-axis is parallel to the direction of core height and the x-axis is perpendicular to the yz-plane.

The mechanical properties of the core are calculated with regard to the homogenization method based on the analytical approach are:

1) Transverse shear modulus in yz-plane (G_{yz})
2) Elastic modulus in y-direction (E_y)
3) Elastic modulus in x-direction (E_x)
4) Transverse shear modulus in xz-plane (G_{xz})
5) In-plane shear modulus (G_{xy})
6) Poisson's ratio in the yx-plane (ν_{yx})
7) The equivalent density (ρ_c)

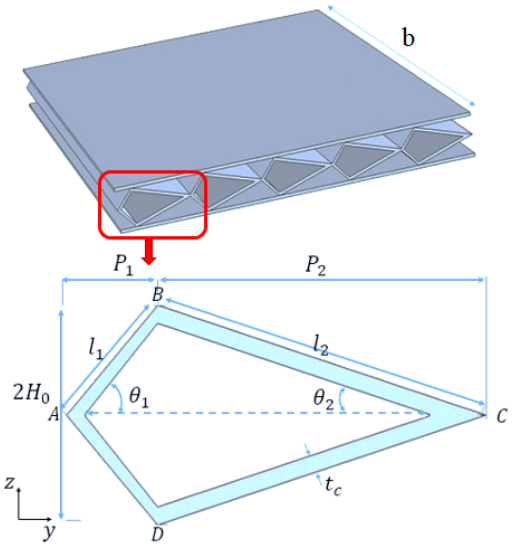

Figure 8 – The geometry of the unit cell

The first parameter of the equivalent material is the transverse shear modulus in the yz plane. The origin of the local coordinate system is set in point A, and the plate is entirely clamped at this point. In pure shear condition, the horizontal force H, a vertical force V, and moment M_0 are applied simultaneously at point B, Figure 9 . The horizontal displacement for shear deformation is calculated while the rotation and vertical displacement at this point are equal to zero, i.e: $\delta_V = 0$, $\delta_{M_0} = 0$.

The inner forces (N, T) and moment (M) at an arbitrary point along the segment AB are expressed as:

$$\begin{cases} M = H(H_0 - y\tan\theta) + V(P_i - y) - M_0 \\ N = H\cos\theta - V\sin\theta \\ T = H\sin\theta + V\cos\theta \end{cases} . \tag{2.10}$$

Applying the Castigliano's theorem (BARTOLOZZI; BALDANZINI; PIERINI,

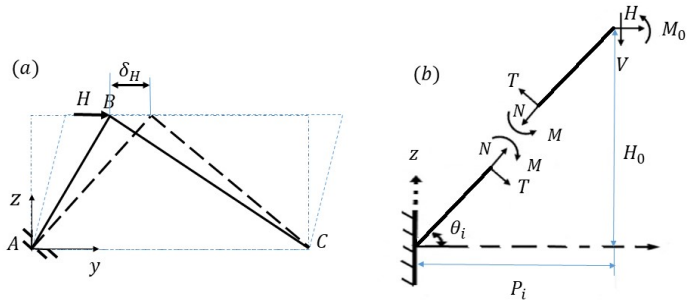

Figure 9 – (a) Pure shear deformation conditions to calculate the G_{yz} parameter (b) The forces analysis diagram on AB segment.

2014) allows obtaining,

$$\begin{cases} \frac{\partial M}{\partial H} = H_0 - y\tan\theta & \frac{\partial M}{\partial V} = P_i - y & \frac{\partial M}{\partial M_0} = -1 \\ \frac{\partial N}{\partial H} = \cos\theta & \frac{\partial N}{\partial V} = -\sin\theta & \frac{\partial N}{\partial M_0} = 0 \\ \frac{\partial T}{\partial H} = \sin\theta & \frac{\partial T}{\partial V} = \cos\theta & \frac{\partial T}{\partial M_0} = 0 \end{cases} , \tag{2.11}$$

$$\begin{cases} \delta_{H_i} = \int_0^{P_i} (\frac{M\frac{\partial M}{\partial H}}{EI} + \frac{N\frac{\partial N}{\partial H}}{EA} + \frac{T\frac{\partial T}{\partial H}}{kGA'})\frac{dy}{cos\theta} \\ \delta_{V_i} = \int_0^{P_i} (\frac{M\frac{\partial M}{\partial V}}{EI} + \frac{N\frac{\partial N}{\partial V}}{EA} + \frac{T\frac{\partial T}{\partial V}}{kGA'})\frac{dy}{cos\theta} \\ \delta_{M_{0i}} = \int_0^{P_i} (\frac{M\frac{\partial M}{\partial M_0}}{EI} + \frac{N\frac{\partial N}{\partial M_0}}{EA} + \frac{T\frac{\partial T}{\partial M_0}}{kGA'})\frac{dy}{cos\theta} \end{cases} , \tag{2.12}$$

where E and G are the Young modulus and shear modulus of the constituent material, respectively, I is the second moment of area, and A is the cross-sectional area and $k = 5/6$ is the shear factor. By substituting Equation (2.11) in (2.12), it results:

$$\begin{bmatrix} \delta_{H_i} \\ \delta_{V_i} \\ \delta_{M_{0i}} \end{bmatrix} = \frac{1}{EA} \begin{bmatrix} C_{11} & C_{12} & C_{13} \\ & C_{22} & C_{23} \\ sym. & & C_{33} \end{bmatrix} \begin{bmatrix} H \\ V \\ M_0 \end{bmatrix} , \tag{2.13}$$

where,

$$\begin{gathered} C_{11} = \frac{12}{t^2}(\frac{H_o^2 P_i}{\cos\theta} + \frac{P_i^3}{3}\frac{\tan^2\theta}{\cos\theta} - \frac{H_0 P_i^2 \tan\theta}{\cos\theta}) + P_i\cos\theta + \frac{2(1+\nu)}{k}(P_i\tan\theta\sin\theta) \quad , \\ C_{12} = \frac{12}{t^2}(\frac{H_0 P_i^2}{2\cos\theta} - \frac{P_i^3\tan\theta}{6\cos\theta}) + (-P_i\sin\theta) + \frac{2(1+\nu)}{k}(P_i\sin\theta) \quad , \\ C_{13} = \frac{12}{t^2}(\frac{P_i^2}{2}\frac{\tan\theta}{\cos\theta} - \frac{H_0 P_i}{\cos\theta}) \quad , \\ C_{22} = \frac{12}{t^2}(\frac{P_i^3}{3\cos\theta}) + (P_i\frac{\sin^2\theta}{\cos\theta}) + \frac{2(1+\nu)}{k}(P_i\cos\theta) \quad , \\ C_{23} = C_{32} = \frac{12}{t^2}(\frac{-P_i^2}{2\cos\theta}) \quad , \\ C_{33} = \frac{12}{t^2}(\frac{P_i}{\cos\theta}) \end{gathered} \tag{2.14}$$

Therefore, by applying the BCs, the horizontal displacement δ_H for the i^{th} segment can be found as:

$$\delta_{H_i} = \frac{1-\nu^2}{EA}\frac{\det(\mathbf{C})}{\det(\mathbf{C}_{red})} \quad , \tag{2.15}$$

which index i denotes the segments AB, BC, AD, and DC, respectively, which are shown in Figure 8, and $\mathbf{C}_{red}$ matrix is defined as:

$$\mathbf{C}_{red} = \begin{bmatrix} C_{22} & C_{23} \\ C_{32} & C_{33} \end{bmatrix} \quad . \tag{2.16}$$

Since segments one and two have the same displacement at the free end under a common force H, they act like two parallel springs. Similarly, segments three and four are two springs in parallel. Considering that $k_{eq_{12}}$ and $k_{eq_{34}}$ can be handled as two springs in parallel, namely:

$$k_{eq12} = k_1 + k_2 = \frac{1}{\delta_{H_1}} + \frac{1}{\delta_{H_2}} = \frac{1}{\delta_{H_{eq12}}} \quad , \tag{2.17}$$

$$k_{eq34} = k_3 + k_4 = \frac{1}{\delta_{H_3}} + \frac{1}{\delta_{H_4}} = \frac{1}{\delta_{H_{eq34}}} \quad , \tag{2.18}$$

$$k_{eq} = k_{eq12} + k_{eq34} = \frac{1}{\delta_{H_{eq12}}} + \frac{1}{\delta_{H_{eq34}}} = \frac{1}{\delta_H} \quad , \tag{2.19}$$

$$G_{yz_{core}} = \frac{\tau_{yz}}{\gamma_{yz}} = \frac{F_y/A_{yx}}{\delta_y/l_z} = \frac{H_0}{P_0}\frac{1}{\delta_H} \quad , \tag{2.20}$$

where k_{eq12} is the equivalent spring constant of segments one and two, and k_{eq34} is the equivalent spring constant of segments three and four. Moreover, Equation (2.19) shows that the total displacement δ_H is obtained as the inverse of the total spring constant K_{eq}.

The second equivalent material parameter is the modulus of elasticity in the longitudinal direction. Following the same procedure seen for G_{yz}, for the computation of E_y the two segments one and two of the core are subjected to a unit horizontal force H and the related horizontal displacements δ_{H_i} are derived for both the segments, namely:

$$\begin{cases} M = H(H_0 - y\tan\theta) - M_0 \\ N = H\cos\theta \\ T = H\sin\theta \end{cases} , \tag{2.21}$$

$$\begin{cases} \frac{\partial M}{\partial H} = H_0 - y\tan\theta & \frac{\partial M}{\partial M_0} = -1 \\ \frac{\partial N}{\partial H} = \cos\theta & \frac{\partial N}{\partial M_0} = 0 \\ \frac{\partial T}{\partial H} = \sin\theta & \frac{\partial T}{\partial M_0} = 0 \end{cases} , \tag{2.22}$$

$$\begin{bmatrix} \delta_{H_i} \\ \delta_{M_{0i}} \end{bmatrix} = \frac{1}{EA}\begin{bmatrix} C_{11} & C_{13} \\ C_{31} & C_{33} \end{bmatrix}\begin{bmatrix} H \\ M_0 \end{bmatrix} \quad , \tag{2.23}$$

$$\delta_{H_i} = \frac{1-\nu^2}{EA}(C_{11} - \frac{c_{13}^2}{c_{33}}) \tag{2.24}$$

Considering segments one and two acting like two springs in a series. Similarly, segments three and four are two springs in a series, too. However, $k_{eq_{12}}$ and $k_{eq_{34}}$ can be handled as two springs in parallel, which results,

$$\delta_{Heq12} = \delta_{H1} + \delta_{H2} \quad , \tag{2.25}$$

$$\delta_{Heq34} = \delta_{H3} + \delta_{H4} \quad , \tag{2.26}$$

$$\frac{1}{\delta_H} = \frac{1}{\delta_{Heq12}} + \frac{1}{\delta_{Heq34}} \quad , \tag{2.27}$$

$$E_{y_{core}} = \frac{\sigma_y}{\epsilon_y} = \frac{F_y/A_{xz}}{\sigma_y/l_y} = \frac{P_0}{H_0}\frac{1}{\delta_H} \quad . \tag{2.28}$$

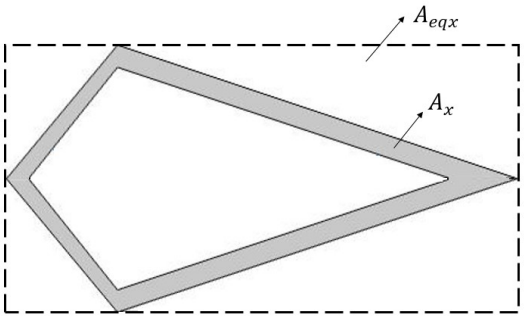

Figure 10 – The equivalent structures area section and section area of plates schematic diagram.

The modulus of elasticity in the lateral direction (x-direction) can be computed as the Young modulus of constituent material E multiplied by the ratio of actual section area of plates and equivalent structures, as shown in Figure 10:

$$E_{x_{core}} = E\frac{A_x}{A_{eq_x}} = E\frac{2t_c(l_1+l_2)}{2H_0P_0} = E\frac{t_c(l_1+l_2)}{H_0P_0} \quad , \tag{2.29}$$

with

$$l_1 = \frac{P_1}{cos(\theta_1)} \ , \quad l_2 = \frac{P_2}{cos(\theta_2)} \tag{2.30}$$

where A_x and A_{eq_x} are the actual section area of the corrugated core sheet and the section area of the equivalent material, and l_1 and l_2 are the length of segments one and two, respectively.

The transverse shear modulus in the xz-plane G_{xz} can be derived for each of the four segments based on considerations done by Bartolozzi, Baldanzini and Pierini (2014). Since both middle ends are supposed to be clamped, the investigated cell can also be part of a periodic structure. Considering again separately the segments one, two, three, and four the formula given by Bartolozzi, Baldanzini and Pierini (2014) can be written for each of them as:

$$G_{xz_i} = G\frac{H_0 t_c}{P_i l_i} \quad . \tag{2.31}$$

As already assumed for the G_{yz} parameter, also in this case the segments one and two and also segments three and four are supposed to work as two springs in parallel since they must have the same displacement of the upper end. Furthermore, the upper equivalent part and the lower equivalent part act like two parallel springs. Skipping the step to obtain the spring stiffness values, it can directly write the equivalent shear modulus as:

$$G_{xz} = G_{xz_1}V_1 + G_{xz_2}V_2 + G_{xz_3}V_3 + G_{xz_4}V_4 \quad , \tag{2.32}$$

where

$$V_i = \frac{P_i}{P_1 + P_2 + P_3 + P_4} \quad . \tag{2.33}$$

Substituting Equations (2.31) and (2.33) in Equation (2.32), gives:

$$G_{xz_{core}} = G\frac{2H_0 t_c}{P_0}(\frac{1}{l_1} + \frac{1}{l_2} + \frac{1}{l_3} + \frac{1}{l_4}) \quad . \tag{2.34}$$

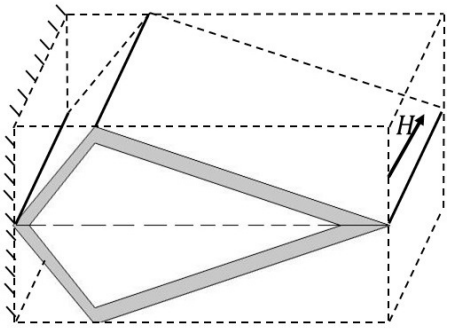

Figure 11 – The scheme of the G_{xy} parameter.

This section involves the calculation of the G_{xy} parameter. In order to estimate this parameter, the left end of the unit cell is clamped and a force H is applied in the x-direction at another end as shown in Figure 11. The displacement of the free end in the x-direction can then be calculated, in pure shear conditions:

$$\delta_{xy12} = \frac{H(l_1 + l_2)}{\frac{5}{6}Gt_c b} \quad , \tag{2.35}$$

$$\delta_{xy34} = \frac{H(l_1 + l_2)}{\frac{5}{6}Gt_c b} \quad , \tag{2.36}$$

$$\frac{1}{\delta_{xyeq}} = \frac{1}{\delta_{xy12}} + \frac{1}{\delta_{xy34}} \quad , \tag{2.37}$$

$$\delta_{xyeq} = \frac{1}{2}\frac{H(l_1 + l_2)}{\frac{5}{6}Gt_c b} \quad . \tag{2.38}$$

Moreover, the shear deformation of the volume occupied by the equivalent material in the period P_0, can be determined as:

$$\delta_{xy_{eq}} = \frac{HP_0}{\frac{5}{6}G_{xy}2H_0 b} \quad . \tag{2.39}$$

By putting these two expressions equal, the value of the G_{xy} can be found as:

$$G_{xy_{core}} = G\frac{t_c}{H_0}\frac{P_0}{(l_1 + l_2)} \quad . \tag{2.40}$$

Assuming the Poisson's ratio in the xy-plane (ν_{xy}) to be equal to that of the constituent material, as typically done by Bartolozzi, Baldanzini and Pierini (2014) and ν_{yx} are:

$$\nu_{xy_{core}} = \nu \quad , \tag{2.41}$$

and

$$\nu_{yx_{core}} = \nu\frac{E_y}{E_x} \quad . \tag{2.42}$$

The mass density of the core is calculated as follows:

$$\rho_{core} = \rho\frac{Lt_c}{P_0 2H_0} \quad , \tag{2.43}$$

where

$$L = l_1 + l_2 + l_3 + l_4 \quad . \tag{2.44}$$

3 AEROELASTIC MODEL AND FLUTTER ANALYSIS

A simply supported rectangular topology optimized core sandwich panel, that the external side is in supersonic airflow, is displayed in Figure 12, with length b, width L which ($L = b$) and height h. The thicknesses of the core, upper and lower face sheets are h_2, h_3, and h_1 respectively. The thickness of the topology-optimized core is t_c. Due to the periodicity and symmetry, the core can be divided into multiple units with the same shape. The x-axis of the reference frame is defined along the corrugation direction and the y-axis denotes the transverse direction where the supersonic airflow comes, while z-direction is perpendicular to the xy-plane.

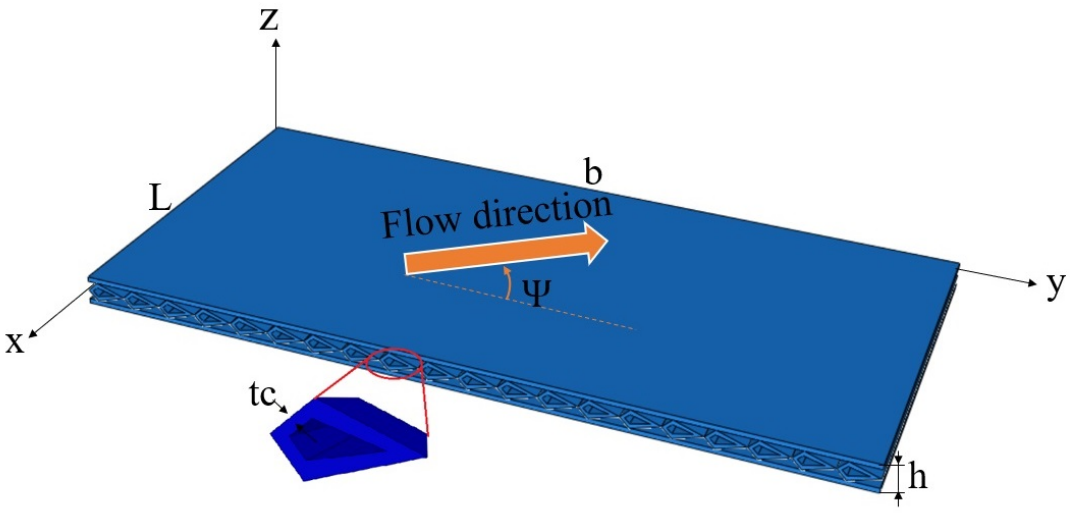

Figure 12 – Supersonic panel flutter problem.

3.1 Structure model

After the homogenization process of topology optimized core, a higher order layerwise theory (FERREIRA, 2005) is used for the displacement field of the equivalent three-layer sandwich panel, as diagrammatically displayed in Figure 13. A higher-order layerwise theory, is utilized for modeling the displacement field of an equivalent three-layer sandwich panel because it offers a more accurate representation of the structural response and behavior of the panel. This type of theory takes into account higher-order deformations, allowing for a more precise prediction of how the layers within the sandwich panel interact and deform under various loading conditions. The use of a higher-order layerwise theory provides better insights into phenomena such as shear and interlaminar stresses, which may not be adequately captured by simpler models. This increased accuracy is especially crucial in applications where structural integrity and performance are paramount, ensuring that

the design and analysis of the sandwich panel are more reliable and closer to real-world behavior (FERREIRA, 2005).

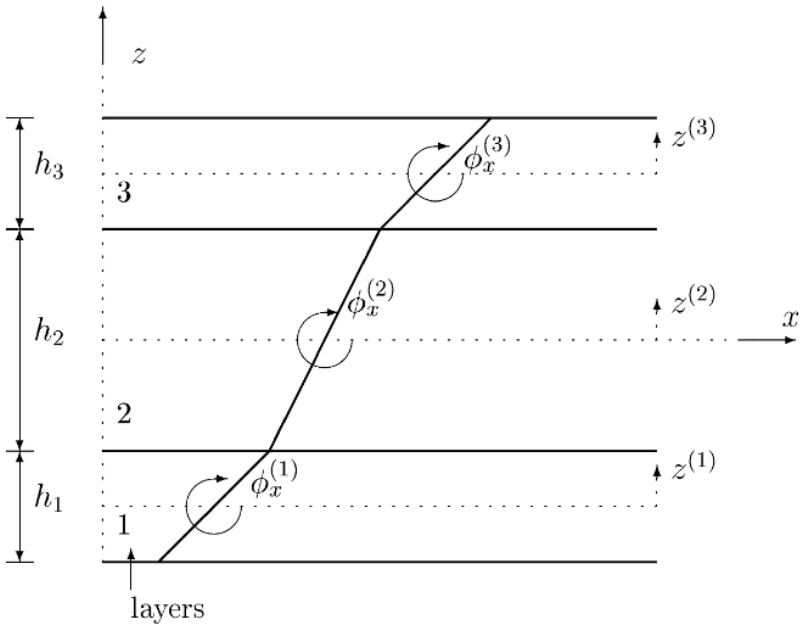

Figure 13 – Depiction of the layerwise kinematics in one dimension (FERREIRA, 2005)

The displacement field in the middle layer (the core in the sandwich plate) is defined as,

$$\begin{cases} u^{(2)}(x,y,z,t) = u_0(x,y,t) + z^{(2)}\phi_x^{(2)}(x,y,t) \\ v^{(2)}(x,y,z,t) = v_0(x,y,t) + z^{(2)}\phi_y^{(2)}(x,y,t) \\ \omega^{(2)}(x,y,z,t) = \omega_0(x,y,t) \end{cases} , \tag{3.1}$$

being u and v the inplane displacements at any point (x, y, z), u_0 and v_0 the in-plane displacement of the point $(x, y, 0)$ on the midplane of the core, ω is the deflection, $\phi_x^{(2)}$, and $\phi_y^{(2)}$ are the rotations. The strain and displacement relation for the middle layer is derived as,

$$\varepsilon^{(2)} = \begin{Bmatrix} \varepsilon_x^{(2)} \\ \varepsilon_y^{(2)} \\ \gamma_{xy}^{(2)} \\ \gamma_{xz}^{(2)} \\ \gamma_{yz}^{(2)} \end{Bmatrix} = \begin{Bmatrix} \frac{\partial u_0}{\partial x} \\ \frac{\partial v_0}{\partial y} \\ \frac{\partial u_0}{\partial y} + \frac{\partial v_0}{\partial x} \\ \frac{\partial \omega_0}{\partial x} + \phi_x^{(2)} \\ \frac{\partial \omega_0}{\partial y} + \phi_y^{(2)} \end{Bmatrix} + z^{(2)} \begin{Bmatrix} \frac{\partial \phi_x^{(2)}}{\partial x} \\ \frac{\partial \phi_y^{(2)}}{\partial y} \\ \frac{\partial \phi_x^{(2)}}{\partial y} + \frac{\partial \phi_y^{(2)}}{\partial x} \\ 0 \\ 0 \end{Bmatrix} , \tag{3.2}$$

The plate strain separates into in-plane strain, ε_p, and transverse shear strain, ε_s and can be expressed as,

$$\varepsilon_p^{(2)} = \begin{Bmatrix} \varepsilon_x^{(2)} \\ \varepsilon_y^{(2)} \\ \gamma_{xy}^{(2)} \end{Bmatrix} = \varepsilon^{m(2)} + z^{(2)}\varepsilon^{f(2)} \quad , \tag{3.3}$$

and

$$\varepsilon_s^{(2)} = \begin{Bmatrix} \gamma_{xz}^{(2)} \\ \gamma_{yz}^{(2)} \end{Bmatrix} \quad , \tag{3.4}$$

in which $\varepsilon^{m(2)}$ and $\varepsilon^{f(2)}$ are the membrane and bending components of the middle layer.

The corresponding displacement fields, strain, and displacement relations for the (skins) upper-layer (index 3) and lower-layer (index 1) are given, respectively, as,

$$\begin{cases} u^{(3)}(x,y,z,t) = u_0(x,y,t) + \frac{h_2}{2}\phi_x^{(2)} + \frac{h_3}{2}\phi_x^{(3)} + z^{(3)}\phi_x^{(3)} \\ v^{(3)}(x,y,z,t) = v_0(x,y,t) + \frac{h_2}{2}\phi_y^{(2)} + \frac{h_3}{2}\phi_y^{(3)} + z^{(3)}\phi_y^{(3)} \\ \omega^{(3)}(x,y,z,t) = \omega_0(x,y,t) \end{cases} \quad , \tag{3.5}$$

$$\varepsilon_p^{(3)} = \varepsilon^{m(3)} + z^{(3)}\varepsilon^{f(3)} + \varepsilon^{mf(3)} \quad , \tag{3.6}$$

$$\begin{cases} u^{(1)}(x,y,z,t) = u_0(x,y,t) - \frac{h_2}{2}\phi_x^{(2)} - \frac{h_1}{2}\phi_x^{(1)} + z^{(1)}\phi_x^{(1)} \\ v^{(1)}(x,y,z,t) = v_0(x,y,t) - \frac{h_2}{2}\phi_y^{(2)} - \frac{h_1}{2}\phi_y^{(1)} + z^{(1)}\phi_y^{(1)} \\ \omega^{(1)}(x,y,z,t) = \omega_0(x,y,t) \end{cases} \quad , \tag{3.7}$$

$$\varepsilon_p^{(1)} = \varepsilon^{m(1)} + z^{(1)}\varepsilon^{f(1)} + \varepsilon^{mf(1)} \quad , \tag{3.8}$$

and the membrane-bending coupling components for layers 3 and 1 are $\varepsilon^{mf(3)}$ and $\varepsilon^{mf(1)}$ respectively.

The equation is discretized using the Classical Finite Element formulation. Here, the four-node Lagrangian quadrilateral element for the panel with 9 degrees of freedom per node $u_0, v_0, \omega_0, \phi_x^{(1)}, \phi_y^{(1)}, \phi_x^{(2)}, \phi_y^{(2)}, \phi_x^{(3)}, \phi_y^{(3)}$, that are grouped into membrane DOFs u_0, v_0, transfer DOF ω_0, rotation DOFs of the normals to the midplane about the y and x axes $\phi_x^{(2)}, \phi_y^{(2)}$, to the upper layer about the y and x axes $\phi_x^{(3)}, \phi_y^{(3)}$ and to the bottom layer about the y and x axes $\phi_x^{(1)}, \phi_y^{(1)}$. Hence, the elemental DOF vector can be written as

$$\begin{aligned} u_m &= \begin{bmatrix} u_1 & v_1 & u_2 & v_2 & u_3 & v_3 & u_4 & v_4 \end{bmatrix}^T \quad , \\ u_\omega &= \begin{bmatrix} \omega_1 & \omega_2 & \omega_3 & \omega_4 \end{bmatrix}^T \quad , \\ u_{\phi(1)} &= \begin{bmatrix} \phi_{x1}^{(1)} & \phi_{y1}^{(1)} & \phi_{x2}^{(1)} & \phi_{y2}^{(1)} & \phi_{x3}^{(1)} & \phi_{y3}^{(1)} & \phi_{x4}^{(1)} & \phi_{y4}^{(1)} \end{bmatrix}^T \quad , \\ u_{\phi(2)} &= \begin{bmatrix} \phi_{x1}^{(2)} & \phi_{y1}^{(2)} & \phi_{x2}^{(2)} & \phi_{y2}^{(2)} & \phi_{x3}^{(2)} & \phi_{y3}^{(2)} & \phi_{x4}^{(2)} & \phi_{y4}^{(2)} \end{bmatrix}^T \quad , \\ u_{\phi(3)} &= \begin{bmatrix} \phi_{x1}^{(3)} & \phi_{y1}^{(3)} & \phi_{x2}^{(3)} & \phi_{y2}^{(3)} & \phi_{x3}^{(3)} & \phi_{y3}^{(3)} & \phi_{x4}^{(3)} & \phi_{y4}^{(3)} \end{bmatrix}^T \quad , \end{aligned} \tag{3.9}$$

in which indices 1 through 4 refer to the elemental nodes.

Using the nodal shape functions the DOFs are interpolated as

$$\begin{aligned}
\omega &= N_{\omega}^{T} u_{\omega} = \textstyle\sum_{i=1}^{n} N_i(\zeta,\eta)\omega_i \\
u &= N_{u}^{T} u_{m} = \textstyle\sum_{i=1}^{n} N_i(\zeta,\eta) u_i \\
\upsilon &= N_{\upsilon}^{T} u_{m} = \textstyle\sum_{i=1}^{n} N_i(\zeta,\eta)\upsilon_i \\
\phi_x^{(1)} &= N_{u}^{T} u_{\phi(1)} = \textstyle\sum_{i=1}^{n} N_i(\zeta,\eta)\phi_{x_i}^{(1)} \\
\phi_y^{(1)} &= N_{\upsilon}^{T} u_{\phi(1)} = \textstyle\sum_{i=1}^{n} N_i(\zeta,\eta)\phi_{y_i}^{(1)} \\
\phi_x^{(2)} &= N_{u}^{T} u_{\phi(2)} = \textstyle\sum_{i=1}^{n} N_i(\zeta,\eta)\phi_{x_i}^{(2)} \\
\phi_y^{(2)} &= N_{\upsilon}^{T} u_{\phi(2)} = \textstyle\sum_{i=1}^{n} N_i(\zeta,\eta)\phi_{y_i}^{(2)} \\
\phi_x^{(3)} &= N_{u}^{T} u_{\phi(3)} = \textstyle\sum_{i=1}^{n} N_i(\zeta,\eta)\phi_{x_i}^{(3)} \\
\phi_y^{(3)} &= N_{\upsilon}^{T} u_{\phi(3)} = \textstyle\sum_{i=1}^{n} N_i(\zeta,\eta)\phi_{y_i}^{(3)}
\end{aligned} \quad , \tag{3.10}$$

where, $N_i(\zeta,\eta)$ are the shape functions of a bilinear four-noded Q4 element, namely,

$$N_{\omega} = \begin{Bmatrix} N_1 & N_2 & N_3 & N_4 \end{Bmatrix}^T \quad ,$$

$$N_{u} = \begin{Bmatrix} N_1 & 0 & N_2 & 0 & N_3 & 0 & N_4 & 0 \end{Bmatrix}^T \quad ,$$

$$N_{\upsilon} = \begin{Bmatrix} 0 & N_1 & 0 & N_2 & 0 & N_3 & 0 & N_4 \end{Bmatrix}^T \quad .$$

The bending strain for the three layers can be defined as:

$$\begin{aligned}
\varepsilon_p^{(1)} &= B_m^{(1)} d^e + Z^{(1)} B_f^{(1)} d^e + B_{mf}^{(1)} d^e \\
\varepsilon_p^{(2)} &= B_m^{(2)} d^e + Z^{(2)} B_f^{(2)} d^e \\
\varepsilon_p^{(3)} &= B_m^{(3)} d^e + Z^{(3)} B_f^{(3)} d^e + B_{mf}^{(3)} d^e
\end{aligned} \quad . \tag{3.11}$$

The shear strain for the first, second, and third layers can be defined as:

$$\varepsilon_{(s)}^{(k)} = B_s^{(k)} d^e \quad , \tag{3.12}$$

where $k = 1, 2, 3$ is the numbering of the layers and,

$$d_e^T = \begin{Bmatrix} u_1 & \upsilon_1 & \omega_1 & \phi_{x1}^{(1)} & \phi_{y1}^{(1)} & \phi_{x1}^{(2)} & \phi_{y1}^{(2)} & \phi_{x1}^{(3)} & \phi_{y1}^{(3)} & \dots \\ \phi_{x4}^{(3)} & \phi_{y4}^{(3)} & & & & & & & & \end{Bmatrix} \quad . \tag{3.13}$$

The membrane, bending, membrane-bending coupling, and shear strain matrices of three layers are obtained by derivation of the shape functions as,

$$B_m^{(2)} = \begin{bmatrix} \frac{\partial N}{\partial x} & 0 & 0 & 0 & 0 & 0 & 0 & 0 & 0 \\ 0 & \frac{\partial N}{\partial y} & 0 & 0 & 0 & 0 & 0 & 0 & 0 \\ \frac{\partial N}{\partial y} & \frac{\partial N}{\partial x} & 0 & 0 & 0 & 0 & 0 & 0 & 0 \end{bmatrix} \quad , \tag{3.14}$$

$$B_f^{(2)} = \begin{bmatrix} 0 & 0 & 0 & 0 & 0 & \frac{\partial N}{\partial x} & 0 & 0 & 0 \\ 0 & 0 & 0 & 0 & 0 & 0 & \frac{\partial N}{\partial y} & 0 & 0 \\ 0 & 0 & 0 & 0 & 0 & \frac{\partial N}{\partial y} & \frac{\partial N}{\partial x} & 0 & 0 \end{bmatrix} \quad , \tag{3.15}$$

$$B_s^{(2)} = \begin{bmatrix} 0 & 0 & \frac{\partial N}{\partial x} & 0 & 0 & N & 0 & 0 & 0 \\ 0 & 0 & \frac{\partial N}{\partial y} & 0 & 0 & 0 & N & 0 & 0 \end{bmatrix} \quad , \tag{3.16}$$

$$B_m^{(1)} = B_m^{(3)} = B_m^{(2)} \quad , \tag{3.17}$$

$$B_f^{(1)} = \begin{bmatrix} 0 & 0 & 0 & \frac{\partial N}{\partial x} & 0 & 0 & 0 & 0 & 0 \\ 0 & 0 & 0 & 0 & \frac{\partial N}{\partial y} & 0 & 0 & 0 & 0 \\ 0 & 0 & 0 & \frac{\partial N}{\partial y} & \frac{\partial N}{\partial x} & 0 & 0 & 0 & 0 \end{bmatrix} \quad , \tag{3.18}$$

$$B_{mf}^{(1)} = \begin{bmatrix} 0 & 0 & 0 & \frac{-h_1}{2}\frac{\partial N}{\partial x} & 0 & \frac{-h_2}{2}\frac{\partial N}{\partial x} & 0 & 0 & 0 \\ 0 & 0 & 0 & 0 & \frac{-h_1}{2}\frac{\partial N}{\partial y} & 0 & \frac{-h_2}{2}\frac{\partial N}{\partial x} & 0 & 0 \\ 0 & 0 & 0 & \frac{-h_1}{2}\frac{\partial N}{\partial y} & \frac{h_1}{2}\frac{\partial N}{\partial x} & \frac{-h_2}{2}\frac{\partial N}{\partial y} & \frac{h_2}{2}\frac{\partial N}{\partial x} & 0 & 0 \end{bmatrix} \quad , \tag{3.19}$$

$$B_s^{(1)} = \begin{bmatrix} 0 & 0 & \frac{\partial N}{\partial x} & N & 0 & 0 & 0 & 0 & 0 \\ 0 & 0 & \frac{\partial N}{\partial y} & 0 & N & 0 & 0 & 0 & 0 \end{bmatrix} \quad , \tag{3.20}$$

$$B_f^{(3)} = \begin{bmatrix} 0 & 0 & 0 & 0 & 0 & 0 & 0 & \frac{\partial N}{\partial x} & 0 \\ 0 & 0 & 0 & 0 & 0 & 0 & 0 & 0 & \frac{\partial N}{\partial y} \\ 0 & 0 & 0 & 0 & 0 & 0 & 0 & \frac{\partial N}{\partial y} & \frac{\partial N}{\partial x} \end{bmatrix} \quad , \tag{3.21}$$

$$B_{mf}^{(3)} = \begin{bmatrix} 0 & 0 & 0 & 0 & 0 & \frac{h_2}{2}\frac{\partial N}{\partial x} & 0 & \frac{h_3}{2}\frac{\partial N}{\partial x} & 0 \\ 0 & 0 & 0 & 0 & 0 & 0 & \frac{h_2}{2}\frac{\partial N}{\partial y} & 0 & \frac{h_3}{2}\frac{\partial N}{\partial y} \\ 0 & 0 & 0 & 0 & 0 & \frac{h_2}{2}\frac{\partial N}{\partial y} & \frac{h_2}{2}\frac{\partial N}{\partial x} & \frac{h_3}{2}\frac{\partial N}{\partial y} & \frac{h_3}{2}\frac{\partial N}{\partial x} \end{bmatrix} \quad , \tag{3.22}$$

$$B_s^{(3)} = \begin{bmatrix} 0 & 0 & \frac{\partial N}{\partial x} & 0 & 0 & 0 & 0 & N & 0 \\ 0 & 0 & \frac{\partial N}{\partial y} & 0 & 0 & 0 & 0 & 0 & N \end{bmatrix} \quad . \tag{3.23}$$

Then, the strain energy function U of the plate is obtained by:

$$U = \frac{1}{2}\int_V (\varepsilon^T \sigma + \gamma^T \tau) dV \quad , \tag{3.24}$$

resulting

$$U(\delta) = \frac{1}{2}\int_{\Omega_{layer1}} (\varepsilon_m^{(1)T} A_1 \varepsilon_m^{(1)} + \varepsilon_m^{(1)T} B_1 \varepsilon_f^{(1)} + \varepsilon_m^{(1)T} A_1 \varepsilon_{mf}^{(1)} + \varepsilon_f^{(1)T} B_1 \varepsilon_m^{(1)} + \varepsilon_f^{(1)T} D_1 \varepsilon_f^{(1)} +$$
$$\varepsilon_f^{(1)T} B_1 \varepsilon_{mf}^{(1)} + \varepsilon_{mf}^{(1)T} A_1 \varepsilon_m^{(1)} + \varepsilon_{mf}^{(1)T} B_1 \varepsilon_f^{(1)} + \varepsilon_{mf}^{(1)T} A_1 \varepsilon_{mf}^{(1)} + \varepsilon_s^{(1)T} D_{s1} \varepsilon_s^{(1)}) d\Omega_{layer1} +$$
$$\frac{1}{2}\int_{\Omega_{layer2}} (\varepsilon_m^{(2)T} A_2 \varepsilon_m^{(2)} + \varepsilon_m^{(2)T} B_2 \varepsilon_f^{(2)} + \varepsilon_f^{(2)T} B_2 \varepsilon_m^{(2)} + \varepsilon_f^{(2)T} D_2 \varepsilon_f^{(2)} + \varepsilon_s^{(2)T} D_{s2} \varepsilon_s^{(2)}) d\Omega_{layer2} +$$
$$\frac{1}{2}\int_{\Omega_{layer3}} (\varepsilon_m^{(3)T} A_3 \varepsilon_m^{(3)} + \varepsilon_m^{(3)T} B_3 \varepsilon_f^{(3)} + \varepsilon_m^{(3)T} A_3 \varepsilon_{mf}^{(3)} + \varepsilon_f^{(3)T} B_3 \varepsilon_m^{(3)} +$$
$$\varepsilon_f^{(3)T} D_3 \varepsilon_f^{(3)} + \varepsilon_f^{(3)T} B_3 \varepsilon_{mf}^{(3)} + \varepsilon_{mf}^{(3)T} A_3 \varepsilon_m^{(3)} + \varepsilon_{mf}^{(3)T} B_3 \varepsilon_f^{(3)} + \varepsilon_{mf}^{(3)T} A_3 \varepsilon_{mf}^{(3)} + \varepsilon_s^{(3)T} D_{s3} \varepsilon_s^{(3)}) d\Omega_{layer3} \quad ,$$

where δ is the vector of degrees of freedom associated to the displacement field in a finite element discretization. The extensional, bending-extensional, and bending stiffness coefficients of three layers $(k = 1, 2, 3)$ are defined as,

$$\{A_k, B_k, D_k\} = \int_{z_k}^{z_{k+1}} [\bar{Q}_p^{(k)}] \left\{1, Z, Z^2\right\} dz \quad , \tag{3.25}$$

and the transverse shear stiffness coefficient is,

$$\{D_{sk}\} = \int_{z_k}^{z_{k+1}} [\bar{Q}_s^{(k)}] \upsilon_i \upsilon_j dz \quad , \tag{3.26}$$

where $(i, j = 4, 5)$, υ_i and υ_j are the transverse shear correction factors for non-uniform shear strain distribution through the plate thickness, and $Q_p^{(k)}$ and $Q_s^{(k)}$ are the constitutive matrices for the $k^{(th)}$ layer, and $(k = 1, 2, 3)$ is the index for the bottom, middle, and upper layers, respectively,

$$Q_p^{(k)} = \begin{bmatrix} Q_{11}^{(k)} & Q_{12}^{(k)} & 0 \\ Q_{12}^{(k)} & Q_{22}^{(k)} & 0 \\ 0 & 0 & Q_{66}^{(k)} \end{bmatrix} \quad , \tag{3.27}$$

$$Q_s^{(k)} = \begin{bmatrix} Q_{44}^{(k)} & 0 \\ 0 & Q_{55}^{(k)} \end{bmatrix} \quad . \tag{3.28}$$

For the middle layer $(k = 2)$, the topology-optimized core is homogenized as an orthotropic plate and the angle between the x-axis of the global coordinate system and the 1-axis of the material coordinate system is zero. The coefficients of the core stiffness matrix are given by:

$$\begin{aligned} Q_{11}^{(2)} &= \frac{E_x^c}{1 - \nu_{xy}^c \nu_{yx}^c} \quad , \\ Q_{22}^{(2)} &= \frac{E_y^c}{1 - \nu_{xy}^c \nu_{yx}^c} \quad , \\ Q_{12}^{(2)} &= \frac{\nu_{xy}^c E_y^c}{1 - \nu_{xy}^c \nu_{yx}^c} \quad , \\ Q_{66}^{(2)} &= G_{xy}^c \quad , \\ Q_{44}^{(2)} &= G_{yz}^c \quad , \\ Q_{55}^{(2)} &= G_{xz}^c \quad . \end{aligned} \tag{3.29}$$

For the bottom and top layers $(k = 1, 3)$, the coefficients of the stiffness matrix are given by:

$$\begin{aligned} Q_{11}^{(k)} &= Q_{22}^{(k)} = \frac{E^f}{1-\nu^f\nu^f} \quad , \\ Q_{12}^{(k)} &= \frac{\nu^f E^f}{1-\nu^f\nu^f} \quad , \\ Q_{66}^{(k)} &= Q_{44}^{(k)} = Q_{55}^{(k)} = G^f = \frac{E^f}{2(1+\nu^f)} \quad , \end{aligned} \tag{3.30}$$

where E^f is the Young modulus and ν^f is the Poisson ratio of the constituent material of the face sheet.

The kinetic energy of the plate is given by:

$$T(\delta) = \frac{1}{2}\int \left\{\bar{p}\left[\dot{u}_0^2 + \dot{v}_0^2 + \dot{\omega}_0^2 + I\left(\dot{\theta}_{x1}^2 + \dot{\theta}_{y1}^2 + \dot{\theta}_{x2}^2 + \dot{\theta}_{y2}^2 + \dot{\theta}_{x3}^2 + \dot{\theta}_{y3}^2\right)\right]\right\} d\Omega \quad , \tag{3.31}$$

where $\bar{p} = \int_{z_k}^{z_{k+1}} \rho(z)dz$ and $I = \int_{z_k}^{z_{k+1}} z^2\rho(z)dz$, $\rho(z)$ is the mass density of the plate, and the work done by the externally applied non-conservative load is:

$$W(\delta) = \int_\Omega \Delta P \omega d\Omega \quad , \tag{3.32}$$

where ΔP is the aerodynamic pressure.

3.2 Aerodynamic model

The supersonic aerodynamic loading over the topology optimized sandwich panel is modeled by the aerodynamic pressure based on first-order, high Mach number approximation to linear potential flow is given by the Ackeret equation (MARQUES; NATARAJAN; FERREIRA, 2017):

$$\Delta P = \frac{\rho_a U_a^2}{\sqrt{M_\infty^2 - 1}}\left(\frac{\partial\omega}{\partial x}cos\Psi + \frac{\partial\omega}{\partial y}sin\Psi\right) \quad , \tag{3.33}$$

where ρ_a, U_a, M_∞, and Ψ are the free stream air density, velocity of air, Mach number, and flow angle, respectively.

3.3 Aeroelastic equation of motion and flutter analysis

The governing equations of modal and aeroelastic analysis of the TOP core sandwich panel are obtained by writing the Lagrange equations of motion given by:

$$\frac{\partial}{\partial t}\left[\frac{\partial\left(T+W-U\right)}{\partial\dot{\delta}_i}\right] - \left[\frac{\partial\left(T+W-U\right)}{\partial\delta_i}\right] = 0, \quad \text{for } i = 1, 2, ..., n \quad , \tag{3.34}$$

where T is the kinetic energy (*cf.* Equation (3.31)), U is the potential (or strain) energy (*cf.* Equation (3.24)), W is work done by the externally applied non-conservative load (*cf.* Equation (3.32)), and δ_i is the generalized coordinate.

In this research, eigenvalue analysis of the state-space model was accomplished to analyze the panel flutter. The governing equations thus obtained are solved using the standard Galerkin procedure (MARQUES; NATARAJAN; FERREIRA, 2017). The dynamical finite element equations of the system are written in matrix form:

$$\mathbf{M}\ddot{\delta} + \left(\mathbf{K} + \lambda\bar{\mathbf{A}}\right)\delta = 0 \quad . \tag{3.35}$$

After substituting the characteristic of the time function, $\ddot{\delta} = -\omega^2\delta$, the following algebraic equation is obtained:

$$\left[\left(\mathbf{K} + \lambda\bar{\mathbf{A}}\right) - \omega^2\mathbf{M}\right]\delta = 0 \quad , \tag{3.36}$$

where $\lambda = \frac{\rho_a U_a^2}{\sqrt{M_\infty^2 - 1}}$, $\mathbf{M}$ is the consistent mass matrix, $\mathbf{K}$ is the stiffness matrix, $\bar{\mathbf{A}}$ is the aerodynamic force matrix, and ω is the natural frequency.

When $\lambda = 0$, the eigenvalue of ω is real and positive, since the stiffness matrix and the mass matrix are symmetric and positive definite. However, the aerodynamic matrix $\bar{\mathbf{A}}$ is asymmetric. The addition of the aerodynamic matrix to the stiffness matrix, makes the system asymmetric and complex eigenvalues are thus expected for $\lambda > 0$. As λ increases monotonically from zero, for a particular pressure, two of the eigenvalues will approach each other and become complex conjugates. This is referred to as coalescence of modes. In this study, $\lambda_{critical}$ is considered to be value at which the first coalescence occurs. Beyond this point, the system is deemed unstable.

4 RESULTS AND DISCUSSION

In order to accomplish the following analysis, the computer program is developed by MATLAB codes. Firstly, the validation of homogenization modification is analyzed. Then, a study on the validation example is done to show the computational ability of the layerwise finite element method. Afterward, the natural frequencies and mode shapes of the topology-optimized (TOP) sandwich panel compare with those from the ABAQUS simulation of a detailed 3D finite element model.

Finally, the aeroelastic properties of the TOP sandwich panel are investigated.

4.1 Model Validation

4.1.1 Homogenization method validation

To validate the results of the theoretical analysis of homogenization, the results are expanded to find the mechanical properties of the core with two face sheets and then compared with FE models in two dimensions which are built and analyzed in an ABAQUS plugin tool for periodic homogenization (OMAIREY; DUNNING; SRIRAMULA, 2019). It was made to calculate the homogenized effective elastic properties of a periodic representative volume element that the user has created (RVE). The plugin determines the homogenized properties of the periodic RVE. It automatically implements the principles of the periodic RVE homogenization method in the software's user interface by categorizing, creating, and linking sets required for achieving deformable periodic boundary surfaces, which can distort and no longer remain plane.

Calculation of the mechanical properties of the whole sandwich panel for homogenization validation:

The elastic constants for the whole sandwich panel are given in the sections below. They are based on the classical lamination theory to combine the contribution of the core and the faces for the in-plane properties (BARTOLOZZI; BALDANZINI; PIERINI, 2014). Here the principal material directions (1, 2, 3) coincide with the (x, y, z) coordinate system. The stiffness matrix quantities of the total panel have the following forms:

$$\mathbf{C}_{total} = \frac{\mathbf{C}_1 t_1 + \mathbf{C}_c H + \mathbf{C}_2 t_2}{t_1 + t_2 + H} \quad , \tag{4.1}$$

where $\mathbf{C}_1$ and $\mathbf{C}_2$ are the stiffness matrices of the bottom and top faces with thickness t_1 and t_2 respectively, and $\mathbf{C}_c$ is the equivalent stiffness of the core with thickness H.

Therefore,

$$\mathbf{C}_{total} = \begin{bmatrix} C_{11} & C_{12} & 0 \\ C_{21} & C_{22} & 0 \\ 0 & 0 & C_{66} \end{bmatrix} \quad , \tag{4.2}$$

where

$$\begin{aligned} C_{11} &= \tfrac{E_{11}}{1-\nu_{12}\nu_{21}} \quad , \\ C_{22} &= \tfrac{E_{22}}{1-\nu_{12}\nu_{21}} \quad , \\ C_{12} = C_{21} &= \tfrac{\nu_{21}E_{11}}{1-\nu_{12}\nu_{21}} = \tfrac{\nu_{12}E_{22}}{1-\nu_{12}\nu_{21}} \quad , \\ C_{66} &= G_{12} \quad . \end{aligned} \tag{4.3}$$

From the research conducted by (LIBOVE; HUBKA, 1951):

$$G_{yx_{total}} = \frac{G_c t_c^2}{A_c} + 2G_f t_f \quad , \tag{4.4}$$

where G_c and G_f are the shear modulus of elasticity of core material and shear modulus of elasticity of face sheet material, respectively, and t_c and t_f are the thickness of corrugated-core sheet and thickness of each face sheet, respectively. A_c is the area, per unit width, of the corrugation cross section perpendicular to the corrugation axis.

For the out-of-plane properties, a series behavior of the layers is supposed, and the total shear modulus can be found as (BARTOLOZZI; BALDANZINI; PIERINI, 2014):

$$G_{xz_{total}} = \frac{t_1 + t_2 + 2H_0}{\frac{t_1+t_2}{G_f} + \frac{2H_0}{G_{xz_c}}} \quad , \tag{4.5}$$

and

$$G_{yz_{total}} = \frac{t_1 + t_2 + 2H_0}{\frac{t_1+t_2}{G_f} + \frac{2H_0}{G_{yz_c}}} \quad , \tag{4.6}$$

where t_1 and t_2 are the lower and upper face sheet thickness, respectively, and G_f is the shear modulus of the face sheet material.

The Poisson's ratio ν_{yx} in an orthotropic material is:

$$\nu_{yx_{total}} = \nu_{xy_{total}} \frac{E_{y_{total}}}{E_{x_{total}}} \quad , \tag{4.7}$$

where $\nu_{xy_{total}}$ is equal the $\nu_{xy_{core}}$.

The density of the whole panel is:

$$\rho_{total} = \frac{\rho[t_c(l_1 + l_2) + (H_0 t_f)]}{P_0 H_0} \quad , \tag{4.8}$$

where ρ is the density of the material and other parameters are dimensions of the unit cell shown in Figure 8.

The results of the ABAQUS plugin are compared with the analytical method. The dimensions and material properties of the Figure 8 are set as follows: $\theta_1 = \pi/3$, $\theta_2 = \pi/6$, $P_1 = 2mm, P_2 = 6mm, t_{core} = 0.5mm, t_1 = t_2 = 1mm, k = 5/6, \nu = 0.34, E = 110GPa$.

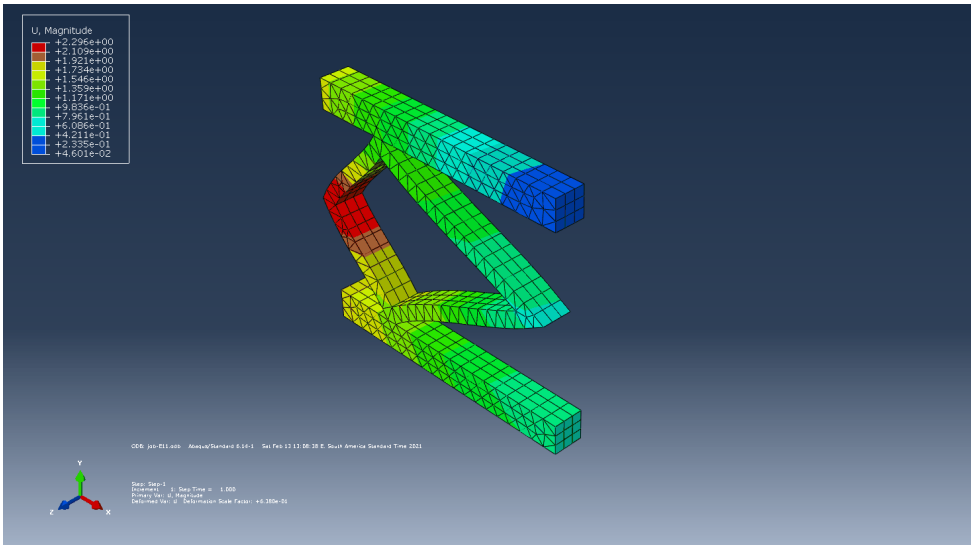

Figure 14 – Model subjected displacements to estimate Young's modulus and Poisson's ratio in x direction

The FEM model of the elastic modulus in x-direction (E_x) and Poisson's ratio (ν_{xy}), is shown in Figure 14.

Figure 15 shows the FEM calculation model of the elastic modulus in y-direction, E_y and Poisson's ratio in y direction ν_{yx}. The FEM model of the transverse shear modulus in xy-plane, G_{xy}, is shown in Figure 16. The FEM model for the transverse shear modulus in xz-plane, G_{xz}, is shown in Figure 17.

The analytical formulation and FE simulation obtain the equivalent beam parameters, and the results of the FE simulation are used to verify the accuracy of analytical formulations. In this section, the mechanical parameters are calculated by these two techniques.

The equivalent properties of the beam are estimated in both analytical and finite element ABAQUS software in Table 2. The results show that the analytical method aligns with the FE simulation, indicating that the analytical approach is suitable for evaluating material parameters in similar structures. However, there are small differences between the analytical approach and the FE models: this is mainly due to the approximation of the analytical method, which considers the center line of the geometry for approximation. Hence, to obtain equivalent parameters for the topology optimized panel, it is sufficient to substitute Young's modulus of the constituent material E with its panel modulus $E/(1-\nu^2)$ in G_{xz} and E_x formulation (BARTOLOZZI; BALDANZINI; PIERINI, 2014). The properties of the isotropic panel and the equivalent properties of the core are estimated in Table 3.

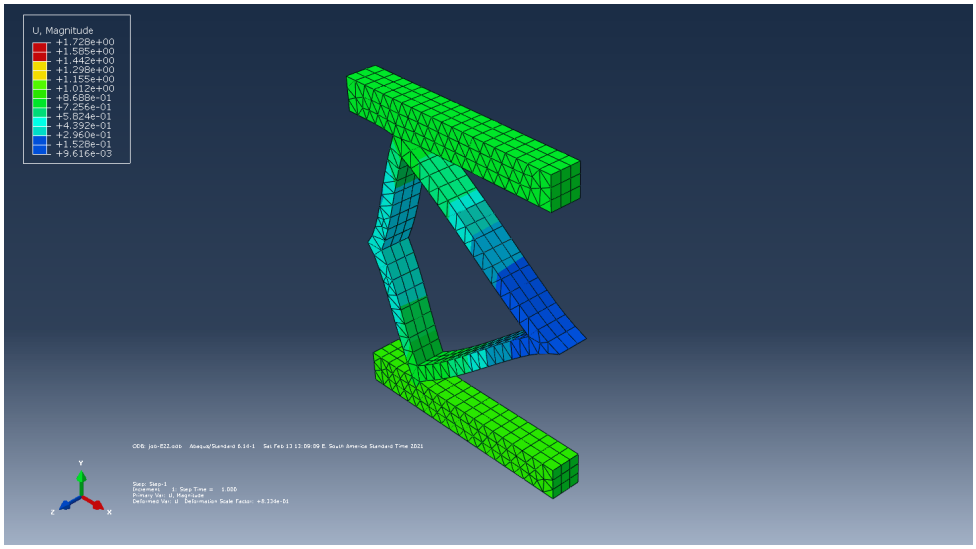

Figure 15 – Model subjected displacements to estimate Young's modulus and Poisson's ratios in y direction

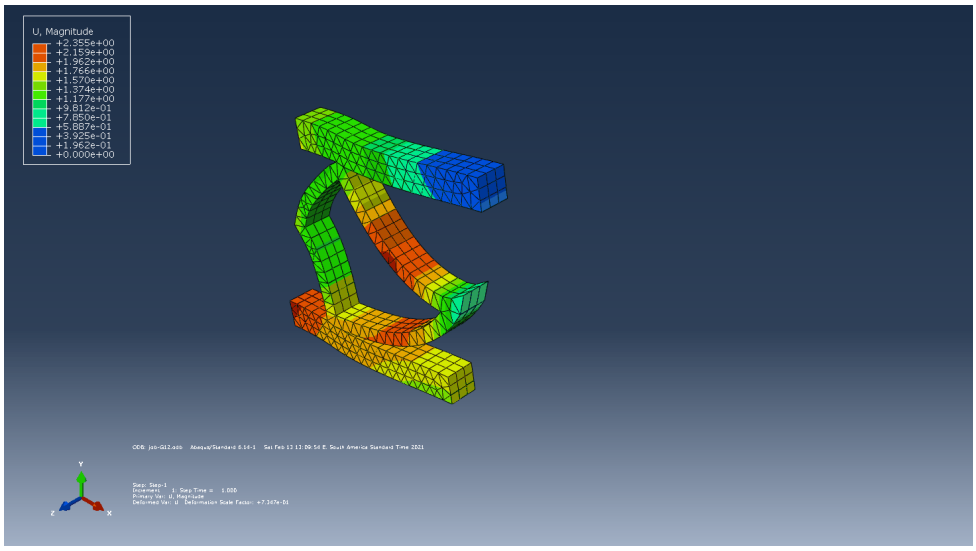

Figure 16 – Model subjected displacements to estimate shear modulus G_{xy}

4.1.2 Layerwise theory validation

In order to study the convergence and accuracy of the present layerwise finite element method, the free vibration problem is performed, and the non-dimensional fundamental frequency, $\Lambda = 100\omega\sqrt{\frac{\rho_{core}h^2}{E_{1core}}}$, given with different mesh sizes of a simply supported square plate is considered in Table 4. The length-to-thickness ratio $(a/h) = 10$, face sheet thicknesses $0.1h$, and core thickness $0.8h$. The material properties for the core and face sheets are as follows:

Core: $E2/E1 = 0.543, G12/E1 = 0.2629, G13/E1 = 0.1599, G23/E1 = 0.2668, \nu = 0.3$.

Facesheets: the material properties of the face sheet are given in terms of the ratio R of those of the core, and R varies from 1 to 10, where the elastic moduli of the face layers

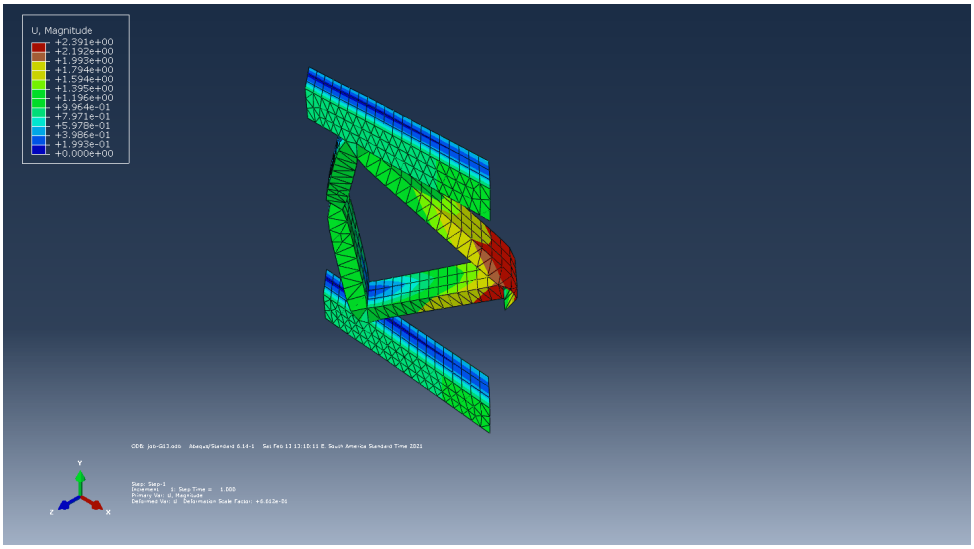

Figure 17 – Model subjected displacements to estimate shear modulus G_{xz}

Table 2 – Comparing equivalent properties of the beam in analytical approach and the FE model.

Mechanical properties	Whole beam (Analytical)	Whole beam (FEM)	Relative difference (%)
$E_x[GPa]$	26.1653	27.0741	-3.36
$E_y[GPa]$	41.4712	41.0656	0.99
$G_{yz}[GPa]$	16.4425	16.1451	1.80
$G_{xy}[GPa]$	15.4743	15.2334	1.55
$G_{xz}[GPa]$	10.0758	10.0152	0.60
ν_{yx}	0.3400	0.3399	0.03
ν_{xy}	0.2145	0.2241	-4.28
$\rho[\frac{g}{cm^3}]$	1.3853	1.4601	-5.39

Table 3 – The properties of the isotropic panel and the equivalent properties of core.

Mechanical properties	Isotropic panel	Core of the panel
$E_x[GPa]$	110	0.5261
$E_y[GPa]$	110	21.6886
$G_{yx}[GPa]$	41.04	4.3369
$G_{yz}[GPa]$	41.04	14.0171
$G_{xy}[GPa]$	41.04	8.0927
$G_{xz}[GPa]$	41.04	9.3558
ν_{yx}	0.34	0.34
ν_{xy}	0.34	0.0082
$\rho[\frac{g}{cm^3}]$	4.3	0.847

are obtained by multiplying R with those of the core.

A mesh convergence analysis is performed on the present model and demonstrates that the 20×20 mesh produces results with satisfactory accuracy. Moreover, the results

obtained by the present method agreed well with the finite element solutions of Chakrabarti and Sheikh (2004).

Table 4 – Convergence study of non-dimensional frequency parameter $\Lambda = 100\omega\sqrt{\frac{\rho_{core}h^2}{E_{1core}}}$ of the present LW model with different mesh sizes.

	R			
Mesh	1	2	5	10
10×10	4.814	6.036	7.860	9.259
12×12	4.834	6.011	7.829	9.223
16×16	4.815	5.988	7.801	9.189
20×20	4.807	5.978	7.788	9.174
25×25	4.802	5.972	7.780	9.165
Chakrabarti and Sheikh (2004)	4.738	5.695	7.695	9.771
Relative errors (%)	1.35	4.86	1.10	-6.20

4.2 Modal analysis of topology optimized core sandwich panel

The TOP sandwich panel, all made of Ti6Al4V alloy, is taken into consideration. The dimensions and material properties of the core and face sheets are set as follows: $L = b, h = 0.01m, L/h = 100, 2H_0 = 0.8h, \theta_1 = \pi/3, \theta_2 = \pi/6, t_{core} = 0.18h, t_s = 0.1h, k = 5/6$, $E = 110GPa, \nu = 0.3, \rho = 4.3g/cm^3$.
Free vibration analysis of the TOP sandwich panel is performed under simply supported at all sides (SSSS). The homogenized TOP sandwich panel is simulated in ABAQUS software by quadratic elements with a total of 2800 elements. The mesh size of the layerwise method is 20×20. The natural frequencies of the first six modes are compared in Table 5. The results calculated by the present method are in good agreement with the solutions of ABAQUS. This comparison reveals the frequencies of low-order modes have good accuracy and validity, and the maximum error of 6.50 percent appears in the sixth mode in modal analysis of the TOP sandwich panel, which indicates that the formulae in this thesis are correct.

Table 5 – Comparison of the present natural frequencies (rad/s) of TOP core sandwich panel under the simple-supported boundary condition (SSSS) with those obtained by the ABAQUS.

Number	Mode shape	Present method	ABAQUS	Relative errors(%)
1	(1,1)	45.59	44.95	1.42
2	(1,2)	104.63	106.76	1.99
3	(2,1)	122.35	118.93	2.87
4	(2,2)	177.76	179.67	-1.06
5	(1,3)	214.47	210.19	2.03
6	(3,1)	258.27	242.49	6.50

The first six mode shapes of the simply supported TOP sandwich panel of the present method and ABAQUS output are displayed in Figure 18 and Figure 19, respectively. The mode shapes from the present method are as same as those from the ABAQUS simulation.

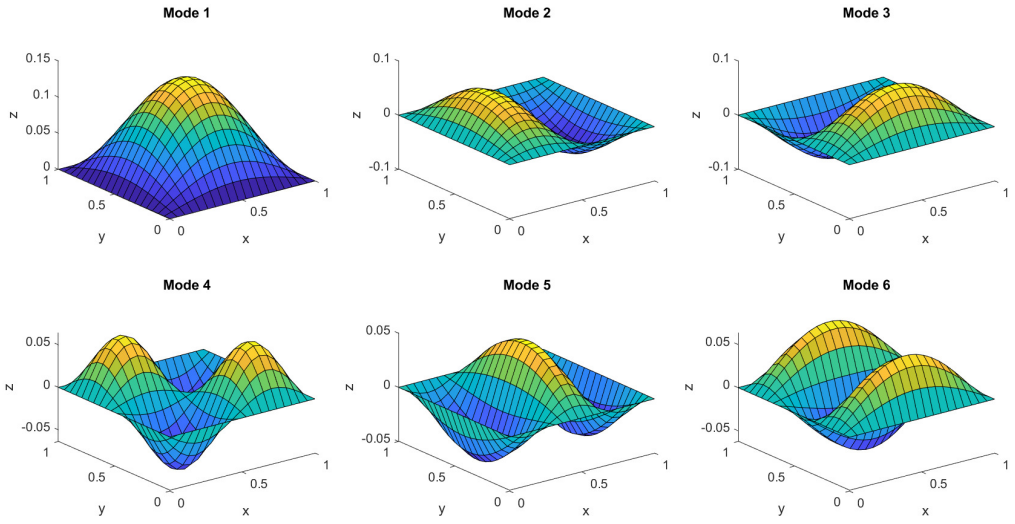

Figure 18 – Mode shapes of the first six order of the simply supported the TOP sandwich panel in the present method.

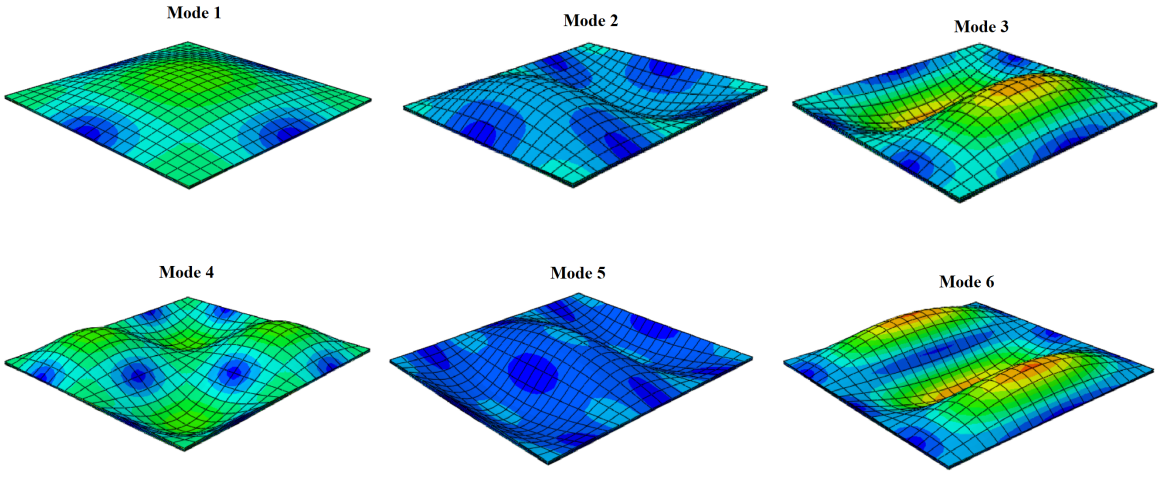

Figure 19 – Mode shapes of the first six order of the simply supported the TOP sandwich panel in ABAQUS.

4.3 Linear flutter analysis of the topology optimized core sandwich panel

Aeroelastic analysis of the TOP sandwich plate listed in Section 4.2 is studied at sea level with air density $\rho_{air} = 1kg/m^3$ and reference Mach number $M_a = 2.0$. The first

four modes of interest are investigated.

The critical flutter λ-Frequency and real to imaginary curves for the simply supported boundary condition are indicated in Figure 20. The flutter, which is widely known to happen when the real part of the eigenvalue shifts from a negative to a positive value, may typically be approximated by the coalescence of two successive natural frequencies. The critical flutter aerodynamic pressure λ_c is the corresponding non-dimensional aerodynamic pressure. From Figure 20, it can be shown that at λ_c=2983, two frequencies coalesce. At λ=2525, the second and third natural frequencies display a veering phenomenon. However, this won't have an impact on the structure's flutter analysis.

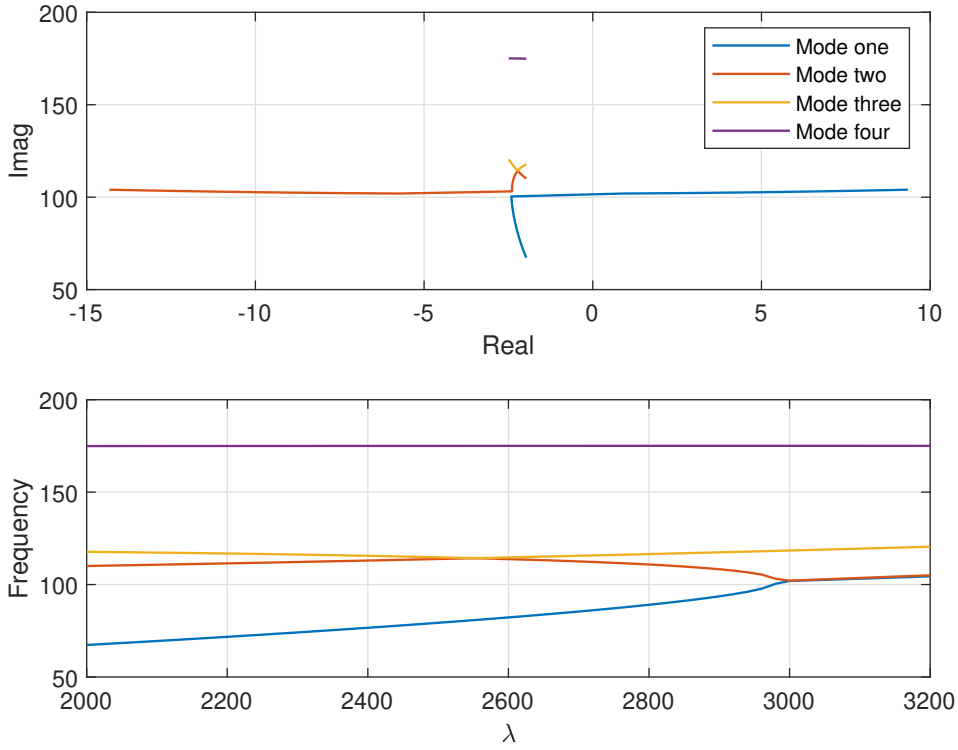

Figure 20 – Critical flutter λ-frequency curve of a TOP sandwich panel with all simply supported sides

The first three orders of mode shapes for various aerodynamic pressures are shown in Figures 21 to 23. Figure 21 shows that the first three orders of mode at λ= 2500 (before the veering point at λ= 2550) are (1, 1), (2, 1), and (1, 2). The first three mode shapes, however, transform after the veering point, at λ_c= 2600, into (1, 1), (1, 2), and (2, 1), Figure 22. The change between modes (2, 1) and (1, 2) shows that the aerodynamic pressure decreases the sandwich panel's rigidity in the y-direction. Additionally, it can be shown in Figure 23 that after the flutter bound, the first two orders of mode shapes become the same.

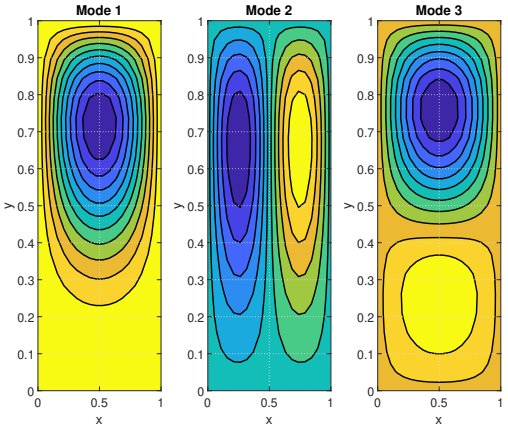

Figure 21 – First three mode shapes under λ= 2500.

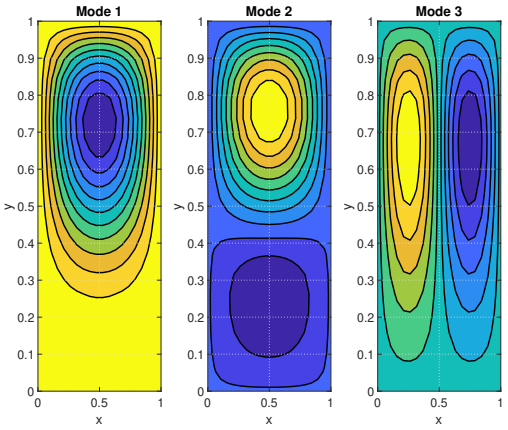

Figure 22 – First three mode shapes under λ= 2600.

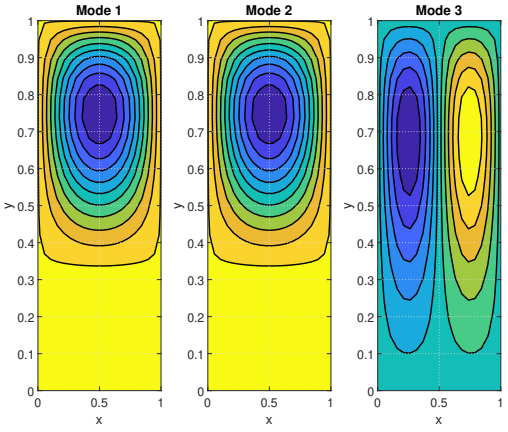

Figure 23 – First three mode shapes under λ= 2990.

4.3.1 Effects of core metastructure thickness

Figure 24 shows the schematic diagram of the TOP unit cell of the core with different thicknesses t_{core}. Except for the core thickness, the geometric and material parameters

of the TOP sandwich panel are the same. Figure 25 displays changes in non-dimensional critical dynamic pressure of the TOP sandwich plates with different thicknesses of the core metastructure. The density of the core rises as metastructure thickness does as well, Figure 26, resulting in higher structural weight and lower critical dynamic pressure.

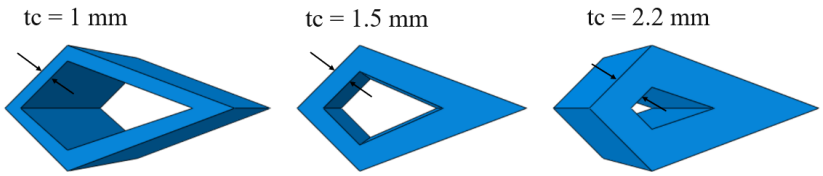

Figure 24 – Schematic diagram of TOP unit cell with different core thickness ratios.

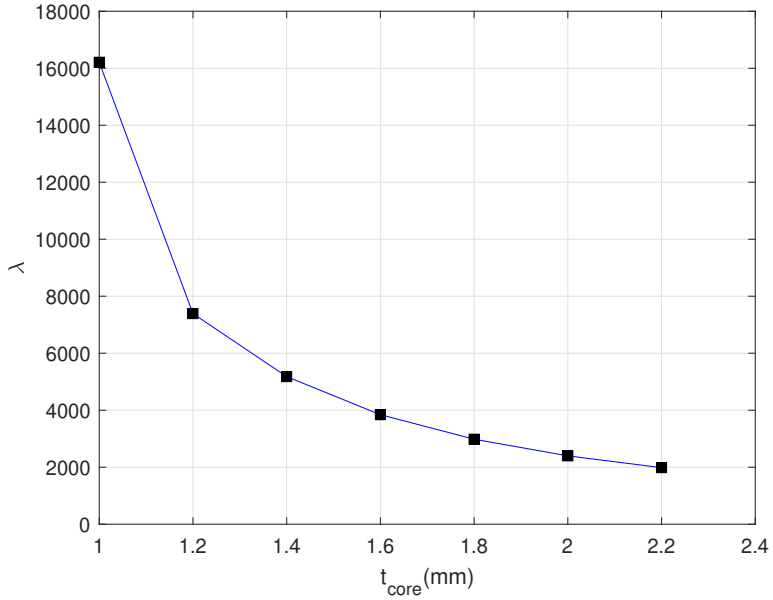

Figure 25 – Effects of core metastructure thickness on nondimensional critical dynamic pressure of a simply supported TOP sandwich panel.

4.3.2 Effects of TOP metastructure angle and face-to-thickness ratio

Figure 28 shows the effects of metastructure angle of the TOP sandwich panel on the non-dimensional critical dynamic pressure λ_c with various θ_2 and θ_1, Figure 27. It is clearly shown that λ_c improves with decreasing the differences between metastructure angles, θ_2 and θ_1. Also, Figure 29 indicates the critical dynamic pressure increases first and then decreases when the thickness of the wall increases. The maximum amount of critical flutter will be in the thickness ratio $t_s/h = 0.15$ with the angles $\theta_1 = \theta_2 = 45$, which shows that the use of geometry inspired by the topology optimization method is an optimum geometry as the core of sandwich panels in aerospace application. In fact, using the topology optimization method in order to minimize compliance and maximize stiffness

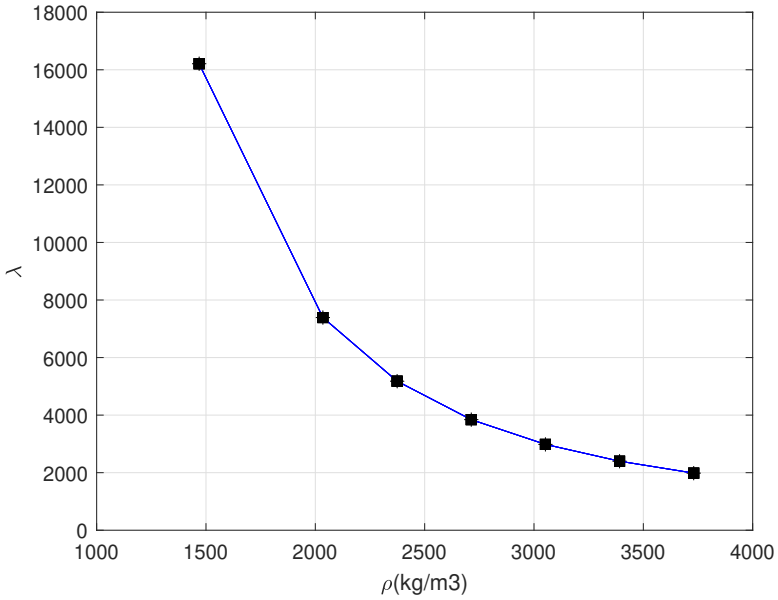

Figure 26 – Effects of core metastructure density on nondimensional critical dynamic pressure of a simply supported TOP sandwich panel.

has a positive effect on the aeroelasticity properties of sandwich panels. Not only does TOP core boost flutter speed, but it also reduces panel weight by 29 percent, improving flight efficiency for the aerospace industry.

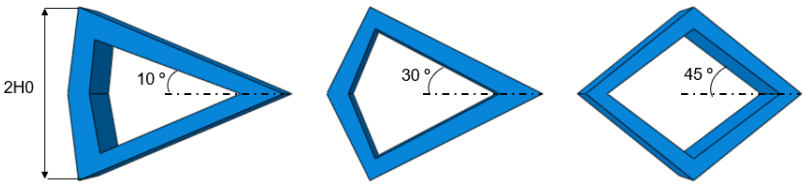

Figure 27 – Schematic diagram of TOP unit cell with different cell angles.

4.3.3 Effects of flow angle

For a TOP sandwich plate with a given side-to-thickness ratio a/h, there are different possible flow angles which is shown in Figure 12, Ψ , with respect to the plane reference system: $0°, 30°, 45°, 60°$, and $90°$. Figure 30 presents the effects of flow angle on the non-dimensional critical dynamic pressure λ_c and flutter frequency. It is shown that the critical flutter aerodynamic pressure decreases as the flow angle rises. The airflow will be oriented in the x-direction when the flow angle equals 90 degrees. The flutter boundaries of the sandwich panel under $0°$ and $90°$ flow angles should be equivalent if the panel's dimensions in the x and y axes are equal since the sandwich panel is transversely isotropic. The sandwich panel under study is a square one with an orthotropic core whose

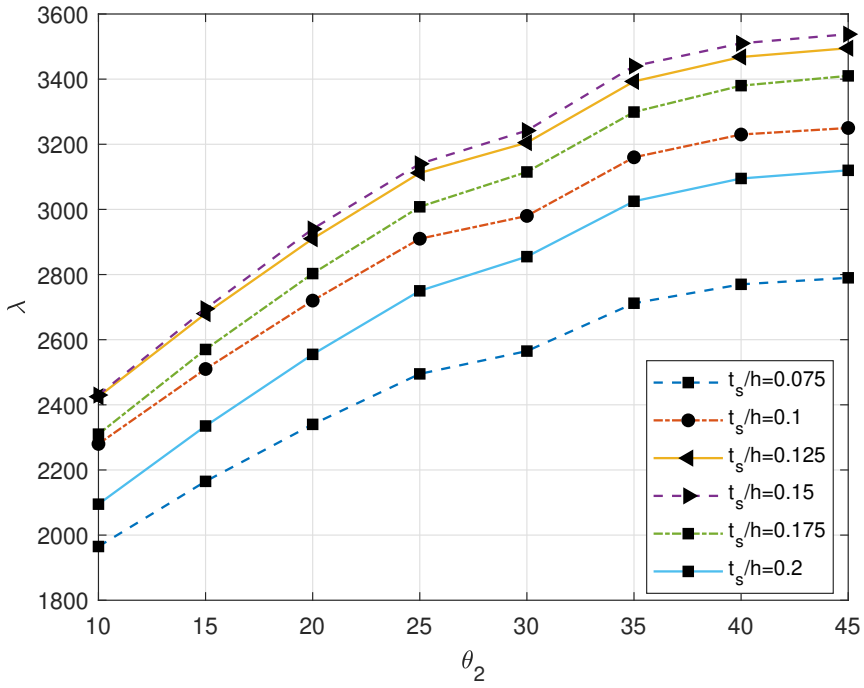

Figure 28 – Effect of cell angle on nondimensional critical dynamic pressure of a simply supported TOP sandwich panel.

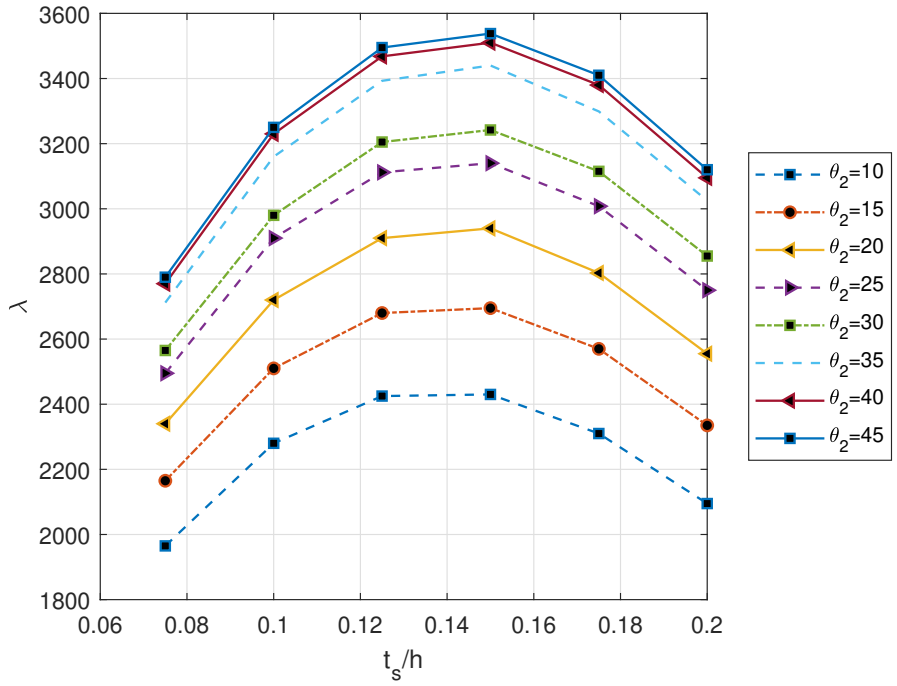

Figure 29 – Effect of ace-to-thickness ratio on nondimensional critical dynamic pressure of a simply supported TOP sandwich panel.

mechanical properties are unique and independent in three overlapping directions. It is the primary reason for the differential results for 0° and 90° flow angles displayed in Figure 30.

Figure 31 displays the sandwich panel's fluttering mode shapes at various flow angles. It is demonstrated how the fluttering mode gradually shifts from (1, 2) to (2, 1).

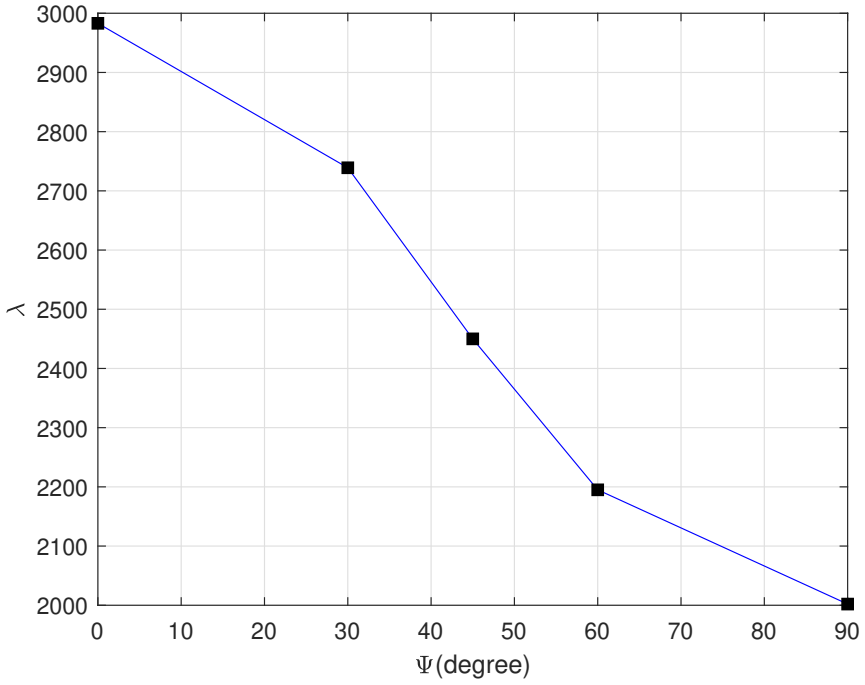

Figure 30 – Effects of flow angle on nondimensional critical dynamic pressure of a simply supported TOP sandwich panel.

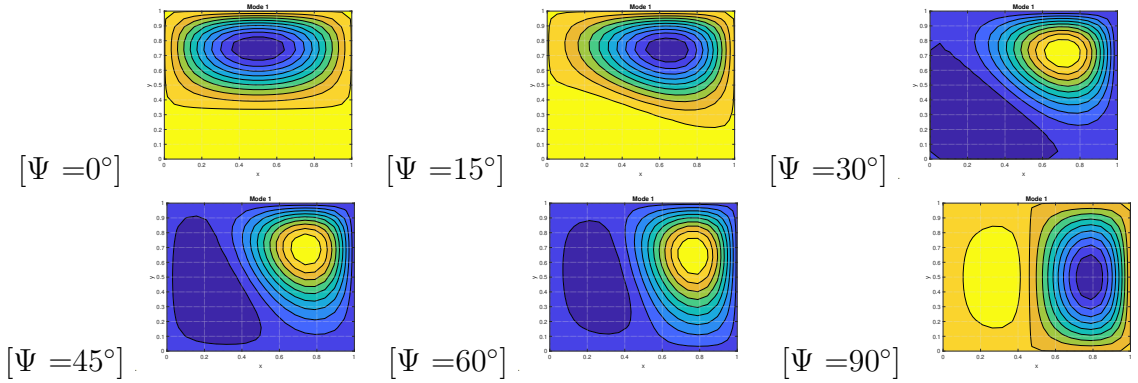

Figure 31 – TOP sandwich panel fluttering modes at different flow angles.

4.3.4 Comparing isotropic panel, isotropic sandwich panel, and TOP sandwich panel

The flutter characteristics of an isotropic panel with the same mass, width, and length as the TOP sandwich panel and a sandwich panel with an isotropic core are examined in order to compare the flutter characteristics of TOP sandwich panels with regular isotropic and sandwich isotropic panels. The formula $h_{iso} = 2h_f + \frac{(\rho_c h_c)}{\rho}$ can be used to get the isotropic panel's thickness.

The natural frequencies of the isotropic panel, isotropic core sandwich panel, and TOP sandwich panel are shown in Figure 32. The results show that in the lower frequencies, the differences between the natural frequencies are less than the ones in the higher ones. While the natural frequencies of the isotropic sandwich panel and isotropic panel are close, the natural frequencies of the TOP sandwich panel are higher with a significant difference.

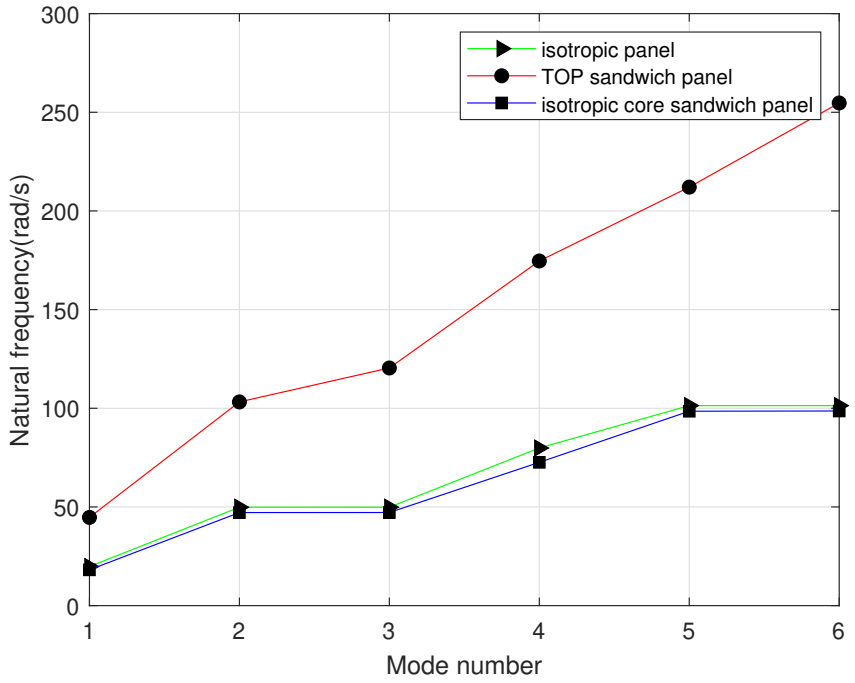

Figure 32 – Comparing natural frequencies of the isotropic panel, Isotropic core sandwich panel, and TOP sandwich panel.

Also, the relationship between natural frequencies and aerodynamic pressure is depicted in Figure 33. The critical flutter aerodynamic pressure of the isotropic panel is $\lambda_c = 520$, which is significantly less than that of the TOP sandwich panel ($\lambda_c = 2983$ as shown in Table 6) while the critical flutter aerodynamic pressure of the sandwich panel with isotropic core is $\lambda_c = 460$ nearly the critical flutter aerodynamic pressure of the isotropic panel with the same density.

Table 6 – Flutter boundaries, thickness, and density of the isotropic, isotropic sandwich, and TOP sandwich panels in the simply supported boundary condition.

	isotropic panel	isotropic core sandwich panel	TOP sandwich panel
λ_c	520	460	2983
$\rho(g/cm^3)$	4.3	4.3	3.0522
$h(mm)$	$2h_f + \frac{(\rho_c h_c)}{\rho} = 7.7$	$2h_f + h_c = 10$	$2h_f + h_c = 10$

The first six shape modes of the panels compared in this section are displayed in Figure 34 through Figure 36.

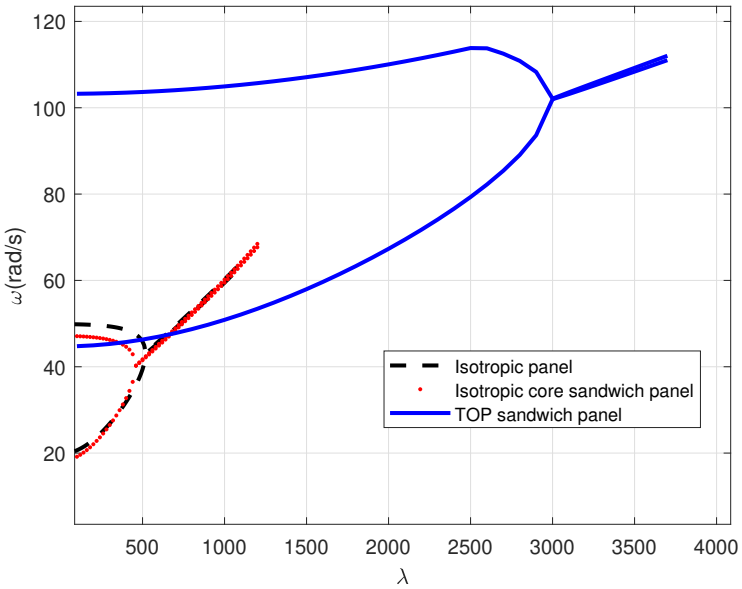

Figure 33 – Comparing variation of aerodynamic pressure of isotropic panel, isotropic core sandwich panel, and TOP sandwich panel.

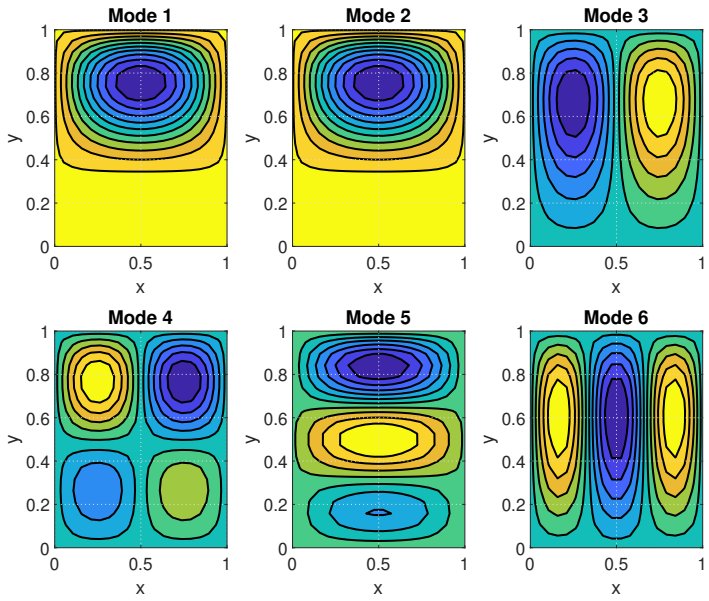

Figure 34 – First six mode shapes of the isotropic panel in flutter condition.

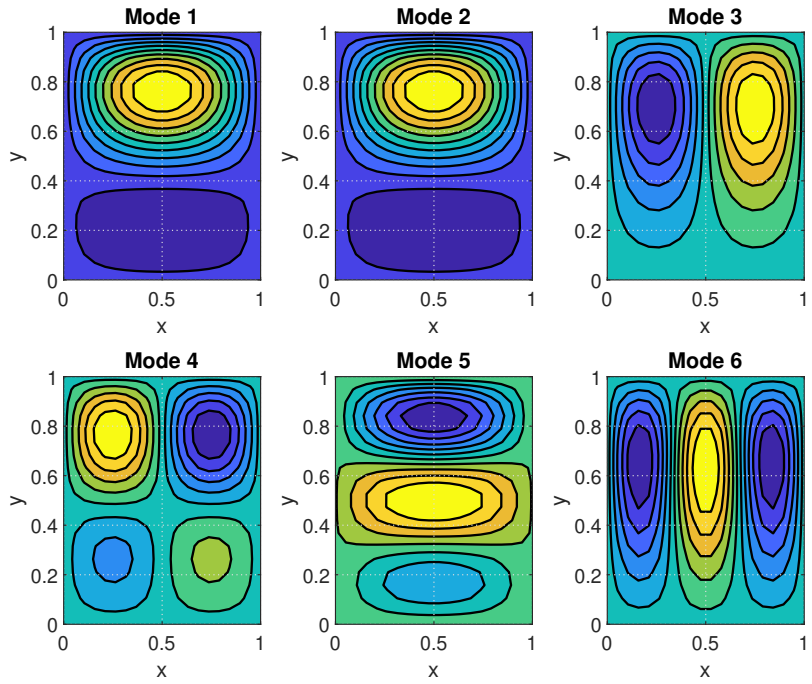

Figure 35 – First six mode shapes of the sandwich panel with the isotropic core in flutter condition.

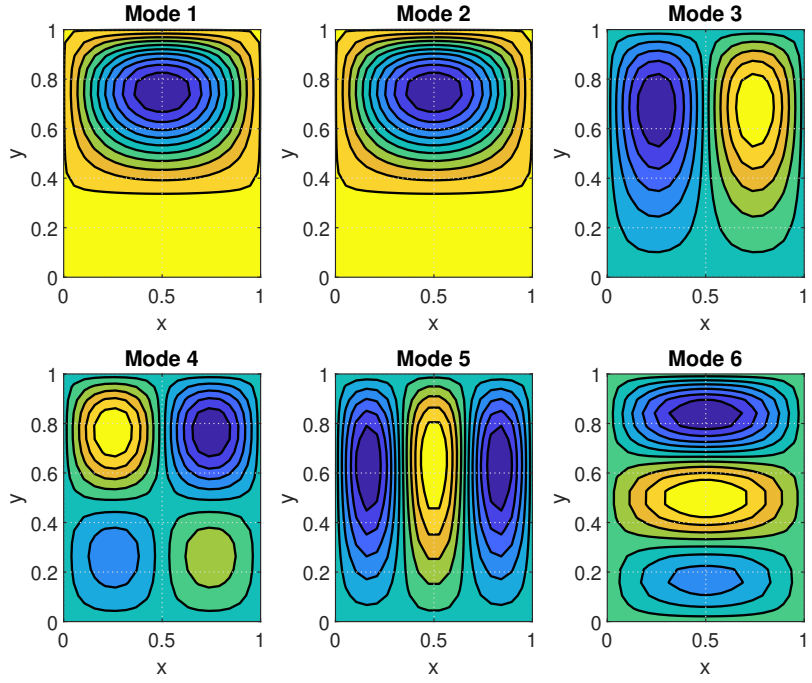

Figure 36 – First six mode shapes of the TOP sandwich panel in flutter condition.

5 CONCLUSIONS AND FUTURE WORKS

5.1 Conclusions

In this research, aeroelastic analysis of a sandwich plate with an inspired topology optimized core is investigated. Firstly, the TOP core is considered a homogeneous continuum with equivalent material properties. A layerwise shear deformation theory with independent rotations in each layer is then applied. Meanwhile, the first-order Piston theory is used to evaluate the aerodynamic load in supersonic flow. Finally, a finite element solution is formulated by adopting a four-noded with 9 degrees of freedom per node.

The variable parameter analysis includes the effects of flow angle, core metastructure thickness and the TOP metastructure angle and face-to-thickness ratio which all affect the critical dynamic pressure of TOP sandwich plates. The main conclusions can be drawn as follows:

1. The topology optimization of the simply supported panel, Figure 7, shows that at the three-quarters of the panel, the topology is thicker and the density of the internal topology of the panel is higher than other parts. It shows the critical point position of the panel in flutter condition that fatigue is happened.

2. In validation of the modified homogenization method, the result in Table 2 shows that the analytical formulation are consistent with those of the FE simulation, which declares that the analytical formulation can be used to analyze the material parameters of equivalent structures better. However, small differences between the analytical approach and the FE models is mainly due to the approximation of the analytical method, which considers the center line of the geometry for approximation.

3. The results indicate corrugation orientates parallel to streamwise lead to better aeroelastic performance.

4. Calculations are made to determine the TOP sandwich plate's critical dynamic pressure of flutter. When the core thickness ratio rises, the critical dynamic pressures fall. When the face sheet thickness increases, the critical dynamic pressure initially rises and then falls. Additionally, λ_c gets better with less of a difference between the angles of the structure. It demonstrates that the aeroelasticity characteristics of sandwich panels are improved by applying the topology optimization approach to minimize compliance and maximize stiffness.

5. The TOP sandwich plate's natural frequencies are contrasted with isotropic panels of equal mass, width, and length as well as with isotropic core sandwich panels of

equal thickness, width, and length, all other plate parameters remaining constant. The natural frequencies of the TOP sandwich panel are higher with a noticeable difference, despite the fact that the natural frequencies of the isotropic sandwich panel and isotropic panel are similar.

6. The critical dynamic pressure of flutter of the TOP sandwich panel, isotropic panel and isotropic core sandwich panel is calculated. The critical flutter aerodynamic pressure of the TOP sandwich panel is significantly higher than that of the isotropic panel, whereas the critical flutter aerodynamic pressure of the sandwich panel with an isotropic core is almost the same as the critical flutter aerodynamic pressure of the isotropic panel with the same density.

7. With comparison the density of isotropic panel, isotropic core sandwich panel and the TOP sandwich panel, the weight of the panel with the new geometry is 29 percent less than the two other ones, which is more lightweight and leads to a decrease in the consumption of fuel and as a results increase the efficiency of the flight.

The present work suggested an efficient metastructure geometry from the topology optimization method as a core of sandwich panels in the aeroelastic application. It is shown that the proposed metastructure has the ability to be used as a lightweight core in aircraft design considering the more critical dimensionless dynamic pressure, which is useful in the research of lightweight sandwich materials applications. Also, the research presented a layer-wise theory approach for sandwich plates with metastructure core for aeroelastic analysis, which can be further developed to considering thermal effect of this type of sandwich panels.

5.2 Future works

This work has investigated the aeroelastic analysis of a sandwich panel that its core is found from 2D topology optimization method.

It would be interesting to investigate the following subjects:

- Studying the aeroelastic behavior of a 3D topology optimized core in flutter condition.
- Studying the aeroelastic analysis of TOP sandwich panel under thermal effects.
- Studying the aeroelastic behavior of multi-bay topology optimized core sandwich panel in flutter condition.
- Studying the nonlinear aeroelasticity of the TOP core Sandwich panel. The unit cell's geometry is expected to influence several properties of the aeroelastic behavior, such as flutter onset condition, LCO amplitude levels, vibration patterns.

- Analyzing the dynamic topology optimization of aeroelasticity problems to maximize the fundamental eigenfrequency.

REFERENCES

ANDREASSEN, E. *et al.* Efficient topology optimization in matlab using 88 lines of code. **Structural and Multidisciplinary Optimization**, Springer, v. 43, n. 1, p. 1–16, 2011.

BARTOLOZZI, G.; BALDANZINI, N.; PIERINI, M. Equivalent properties for corrugated cores of sandwich structures: A general analytical method. **Composite Structures**, Elsevier, v. 108, p. 736–746, 2014.

BENDSØE, M. **e Sigmund, O.(2003). Topology Optimization-Theory, Methods and Applications**. [*S.l.: s.n.*]: Springer, Berlin, 2003.

BENDSOE, M. P.; KIKUCHI, N. Generating optimal topologies in structural design using a homogenization method. **Computer Methods in Applied Mechanics and Engineering.**, Elsevier, p. 71(2):197–224, 1988.

BENDSOE, M. P.; SIGMUND, O. **Topology optimization: theory, methods, and applications**. [*S.l.: s.n.*]: Springer Science & Business Media, 2013.

BHATE, D. *et al.* Classification and selection of cellular materials in mechanical design: Engineering and biomimetic approaches. **Designs**, Multidisciplinary Digital Publishing Institute, v. 3, n. 1, p. 19, 2019.

BISMARCK-NASR, M. N. Finite element method applied to the supersonic flutter of circular cylindrical shells. **International Journal for Numerical Methods in Engineering**, Wiley Online Library, v. 10, n. 2, p. 423–435, 1976.

BISPLINGHOFF, R. L.; ASHLEY, H. **Principles of aeroelasticity**. [*S.l.: s.n.*]: Courier Corporation, 2013.

CASTANIÉ, B.; BOUVET, C.; GINOT, M. Review of composite sandwich structure in aeronautic applications. **Composites Part C: Open Access**, Elsevier, v. 1, p. 100004, 2020.

CHAI, Y.-Y.; SONG, Z.-G.; LI, F.-M. Investigations on the influences of elastic foundations on the aerothermoelastic flutter and thermal buckling properties of lattice sandwich panels in supersonic airflow. **Acta Astronautica**, Elsevier, v. 140, p. 176–189, 2017.

CHAKRABARTI, A.; SHEIKH, A. Vibration of laminate-faced sandwich plate by a new refined element. **Journal of Aerospace Engineering**, American Society of Civil Engineers, v. 17, n. 3, p. 123–134, 2004.

CHENG, Q. H.; LEE, H. P.; LU, C. A numerical analysis approach for evaluating elastic constants of sandwich structures with various cores. **Composite Structures**, Elsevier, v. 74, n. 2, p. 226–236, 2006.

CLAUSEN, A. *et al.* Topology optimized architectures with programmable poisson's ratio over large deformations. **Advanced Materials**, Wiley Online Library, v. 27, n. 37, p. 5523–5527, 2015.

DOWELL, E. H. **Aeroelasticity of plates and shells**. [*S.l.: s.n.*]: Springer Science & Business Media, 1974. v. 1.

FERRARI, F.; SIGMUND, O. A new generation 99 line matlab code for compliance topology optimization and its extension to 3d. **arXiv preprint arXiv:2005.05436**, 2020.

FERREIRA, A. Analysis of composite plates using a layerwise theory and multiquadrics discretization. **Mechanics of Advanced Materials and Structures**, Taylor & Francis, v. 12, n. 2, p. 99–112, 2005.

FINDEISEN, C. *et al.* Characteristics of mechanical metamaterials based on buckling elements. **Journal of the Mechanics and Physics of Solids**, Elsevier, v. 102, p. 151–164, 2017.

FUNG, Y. C. **An introduction to the theory of aeroelasticity**. [*S.l.: s.n.*]: Courier Dover Publications, 2008.

GAO, J. *et al.* Topology optimization for auxetic metamaterials based on isogeometric analysis. **Computer Methods in Applied Mechanics and Engineering**, Elsevier, v. 352, p. 211–236, 2019.

GUEDES, J.; KIKUCHI, N. Preprocessing and postprocessing for materials based on the homogenization method with adaptive finite element methods. **Computer Methods in Applied Mechanics and Engineering**, Elsevier, v. 83, n. 2, p. 143–198, 1990.

GUO, S. Aeroelastic optimization of an aerobatic aircraft wing structure. **Aerospace Science and Technology**, Elsevier, v. 11, n. 5, p. 396–404, 2007.

HE, Z.; XIAO, X.; LI, E. Design for structural vibration suppression in laminate acoustic metamaterials. **Composites Part B: Engineering**, Elsevier, v. 131, p. 237–252, 2017.

KATSIKADELIS, J.; BABOUSKOS, N. Optimum design of thick laminated anisotropic plates via frequency regulation. a bem approach. *In*: **Advances in Mechanics of Materials and Structural Analysis**. [*S.l.: s.n.*]: Springer, 2018. p. 223–239.

KROG, L. *et al.* Topology optimisation of aircraft wing box ribs. *In*: **10th AIAA/ISSMO multidisciplinary analysis and optimization conference**. [*S.l.: s.n.*], 2004. p. 4481.

LEON, D. D. *et al.* Aeroelastic tailoring using fiber orientation and topology optimization. **Structural and Multidisciplinary Optimization**, Springer, v. 46, n. 5, p. 663–677, 2012.

LI, J.; NARITA, Y. Multi-objective design for aeroelastic flutter of laminated shallow shells under variable flow angles. **Composite Structures**, Elsevier, v. 111, p. 530–539, 2014.

LI, Y. *et al.* Design of mechanical metamaterials for simultaneous vibration isolation and energy harvesting. **Applied Physics Letters**, AIP Publishing, v. 111, n. 25, p. 251903, 2017.

LIBOVE, C.; HUBKA, R. E. Elastic constants for corrugated-core sandwich plates. 1951.

MARQUES, F. D.; NATARAJAN, S.; FERREIRA, A. J. Evolutionary-based aeroelastic tailoring of stiffened laminate composite panels in supersonic flow regime. **Composite Structures**, Elsevier, v. 167, p. 30–37, 2017.

MUC, A.; FLIS, J. Closed form solutions–analysis and optimal design of supersonic composite laminated flat plates considering mechanical and thermal effects. **Composite Structures**, Elsevier, v. 230, p. 111491, 2019.

NJUGUNA, J. Flutter prediction, suppression and control in aircraft composite wings as a design prerequisite: A survey. **Structural Control and Health Monitoring: The Official Journal of the International Association for Structural Control and Monitoring and of the European Association for the Control of Structures**, Wiley Online Library, v. 14, n. 5, p. 715–758, 2007.

NOUH, M.; ALDRAIHEM, O.; BAZ, A. Wave propagation in metamaterial plates with periodic local resonances. **Journal of Sound and Vibration**, Elsevier, v. 341, p. 53–73, 2015.

OMAIREY, S. L.; DUNNING, P. D.; SRIRAMULA, S. Development of an abaqus plugin tool for periodic rve homogenisation. **Engineering with Computers**, Springer, v. 35, n. 2, p. 567–577, 2019.

OSANOV, M.; GUEST, J. K. Topology optimization for architected materials design. **Annual Review of Materials Research**, Annual Reviews, v. 46, p. 211–233, 2016.

PACHECO, D. R.; FERREIRA, A. J.; MARQUES, F. D. On the effects of structural coupling on the supersonic flutter and limit cycle oscillations of transversely reinforced panels. **Journal of Fluids and Structures**, Elsevier, v. 79, p. 158–170, 2018.

PENG, H.; PAI, P. F.; DENG, H. Acoustic multi-stopband metamaterial plates design for broadband elastic wave absorption and vibration suppression. **International Journal of Mechanical Sciences**, Elsevier, v. 103, p. 104–114, 2015.

PIDAPARTI, R.; CHANG, C. Finite element supersonic flutter analysis of skewed and cracked composite panels. **Computers & structures**, Elsevier, v. 69, n. 2, p. 265–270, 1998.

SAMANTA, A.; MUKHOPADHYAY, M. Finite element static and dynamic analyses of folded plates. **Engineering structures**, Elsevier, v. 21, n. 3, p. 277–287, 1999.

SHAMONINA, E.; SOLYMAR, L. Metamaterials: How the subject started. **Metamaterials**, Elsevier, v. 1, n. 1, p. 12–18, 2007.

SIGMUND, O. Materials with prescribed constitutive parameters: an inverse homogenization problem. **International Journal of Solids and Structures**, Elsevier, v. 31, n. 17, p. 2313–2329, 1994.

SIGMUND, O. A 99 line topology optimization code written in matlab. **Structural and multidisciplinary optimization**, Springer, v. 21, n. 2, p. 120–127, 2001.

SIGMUND, O.; MAUTE, K. Topology optimization approaches: A comparative review. **Structural and Multidisciplinary Optimization**, Springer, v. 48, n. 6, p. 1031–1055, 2013.

SONG, Z.-G.; LI, F.-M. Aerothermoelastic analysis of lattice sandwich composite panels in supersonic airflow. **Meccanica**, Springer, v. 51, n. 4, p. 877–891, 2016.

SONG, Z.-G.; LI, F.-M. Flutter and buckling characteristics and active control of sandwich panels with triangular lattice core in supersonic airflow. **Composites Part B: Engineering**, Elsevier, v. 108, p. 334–344, 2017.

SONG, Z.-G. *et al.* A new method of smart and optimal flutter control for composite laminated panels in supersonic airflow under thermal effects. **Journal of Sound and Vibration**, Elsevier, v. 414, p. 218–232, 2018.

STANFORD, B.; BERAN, P. Optimal structural topology of a platelike wing for subsonic aeroelastic stability. **Journal of Aircraft**, v. 48, n. 4, p. 1193–1203, 2011.

STANFORD, B.; BERAN, P. Aerothermoelastic topology optimization with flutter and buckling metrics. **Structural and Multidisciplinary Optimization**, Springer, v. 48, n. 1, p. 149–171, 2013.

STRGANAC, T. W.; KIM, Y. I. Aeroelastic behavior of composite plates subject to damage growth. **Journal of Aircraft**, v. 33, n. 1, p. 68–73, 1996.

SUTRADHAR, A. *et al.* Designing patient-specific 3d printed craniofacial implants using a novel topology optimization method. **Medical & biological engineering & computing**, Springer, v. 54, p. 1123–1135, 2016.

VALDEVIT, L.; HUTCHINSON, J. W.; EVANS, A. G. Structurally optimized sandwich panels with prismatic cores. **International Journal of Solids and Structures**, Elsevier, v. 41, n. 18-19, p. 5105–5124, 2004.

VALDEVIT, L. *et al.* Structural performance of near-optimal sandwich panels with corrugated cores. **International Journal of Solids and Structures**, Elsevier, v. 43, n. 16, p. 4888–4905, 2006.

VIJAY, B.; DURVASULA, S. Supersonic flutter of composite skin panels of repeated-sublaminate layup. **Composite Structures**, Elsevier, v. 41, n. 2, p. 121–135, 1998.

WANG, F. Systematic design of 3d auxetic lattice materials with programmable poisson's ratio for finite strains. **Journal of the Mechanics and Physics of Solids**, Elsevier, v. 114, p. 303–318, 2018.

WANG, F.; SIGMUND, O.; JENSEN, J. S. Design of materials with prescribed nonlinear properties. **Journal of the Mechanics and Physics of Solids**, Elsevier, v. 69, p. 156–174, 2014.

WANG, H.-X.; CHUNG, S. W. Equivalent elastic constants of truss core sandwich plates. **Journal of pressure vessel technology**, American Society of Mechanical Engineers Digital Collection, v. 133, n. 4, 2011.

WANG, Y. *et al.* Topological shape optimization of microstructural metamaterials using a level set method. **Computational Materials Science**, Elsevier, v. 87, p. 178–186, 2014.

WEI, Z.; YAM, L.; CHENG, L. Detection of internal delamination in multi-layer composites using wavelet packets combined with modal parameter analysis. **Composite Structures**, Elsevier, v. 64, n. 3-4, p. 377–387, 2004.

WU, W. *et al.* Mechanical design and multifunctional applications of chiral mechanical metamaterials: A review. **Materials & Design**, Elsevier, p. 107950, 2019.

YU, X. *et al.* Mechanical metamaterials associated with stiffness, rigidity and compressibility: A brief review. **Progress in Materials Science**, Elsevier, v. 94, p. 114–173, 2018.

ZHANG, J.; YAN, Z.; XIA, L. Vibration and flutter of a honeycomb sandwich plate with zero poisson's ratio. **Mathematics**, Multidisciplinary Digital Publishing Institute, v. 9, n. 19, p. 2528, 2021.

ZHUANG, W.-Z.; YANG, C.; WU, Z.-G. Aeroelastic analysis of foam-filled composite corrugated sandwich plates using a higher-order layerwise model. **Composite Structures**, Elsevier, v. 257, p. 112996, 2021.


EESC • USP